

Fundamental parameters and abundances of metal-poor stars: the SDSS standard BD +17 4708^{*}

I. Ramírez, C. Allende Prieto, S. Redfield^{**}, and D. L. Lambert

McDonald Observatory and Department of Astronomy, University of Texas at Austin, RLM 15.306 Austin, TX, 78712-1083, USA
e-mail: [ivan;callende;redfield;dll]@astro.as.utexas.edu

Received 22 May 2006 / Accepted 21 August 2006

ABSTRACT

The atmospheric parameters and iron abundance of the *Sloan Digital Sky Survey* (SDSS) spectrophotometric standard star BD +17 4708 are critically examined using up-to-date Kurucz model atmospheres, LTE line formation calculations, and reliable atomic data. We find $T_{\text{eff}} = 6141 \pm 50$ K, $\log g = 3.87 \pm 0.08$, and $[\text{Fe}/\text{H}] = -1.74 \pm 0.09$. The line-of-sight interstellar reddening, bolometric flux, limb-darkened angular diameter, stellar mass, and the abundances of Mg, Si, and Ca are also obtained: $E(B-V) = 0.010 \pm 0.003$, $f_{\text{bol}} = (4.89 \pm 0.10) \times 10^{-9}$ erg cm⁻² s⁻¹, $\theta = 0.1016 \pm 0.0023$ mas, $M = 0.91 \pm 0.06 M_{\odot}$, $[\text{Mg}/\text{Fe}] = 0.40 \pm 0.10$, $[\text{Si}/\text{Fe}] = 0.35 \pm 0.11$, $[\text{Ca}/\text{Fe}] = 0.36 \pm 0.11$. This star is a unique example of a moderately metal-poor star for which the effective temperature (T_{eff}) can be accurately constrained from the *observed* spectral energy distribution (corrected for reddening). Such analysis leads to a value that is higher than most spectroscopic results previously reported in the literature (~ 5950 K). Interstellar reddening was estimated using various prescriptions, including an analysis of interstellar lines. The surface gravity of the star was inferred from the fitting of the wings of the Mg I b lines. We used transition probabilities measured in the laboratory and reliable damping constants for unblended Fe lines to derive the iron abundance using both Fe I and Fe II lines. We find that the ionization balance of Fe lines is satisfied only if a low T_{eff} (~ 5950 K) is adopted. The mean iron abundance we obtain from the Fe II lines corresponds to $A_{\text{Fe}} = 5.77 \pm 0.09$ ($[\text{Fe}/\text{H}] = -1.74$ for our derived $A_{\text{Fe},\odot} = 7.51$) while that from the Fe I lines is $A_{\text{Fe}} = 5.92 \pm 0.11$, and therefore with our preferred T_{eff} (6141 K), the discrepancy between the mean iron abundance from Fe I and Fe II lines cannot be explained by overionization by UV photons as the main non-LTE effect. Interestingly, the Fe I excitation balance is satisfied with a T_{eff} only slightly warmer than our preferred solution and not with the lower value of 5950 K. We also comment on non-LTE effects and the importance of inelastic collisions with neutral H atoms in the determination of oxygen abundances in metal-poor stars from the 7774 Å O I triplet.

Key words. stars: abundances – stars: fundamental parameters – stars: individual: BD +17 4708

1. Introduction

The derivation of stellar chemical compositions relies on the accurate determination of the atmospheric parameters T_{eff} (effective temperature) and $\log g$ (surface gravity). These quantities may be inferred either from the stellar spectrum or by semi-empirical methods that are normally based on photometric and astrometric measurements. Often, the photometric and astrometric parameters are used as first approximations and the final solution is found iteratively with the help of the spectrum. This tuning of parameters is, however, model-dependent, and may lead to erroneous conclusions if the models are inadequate.

Most abundance analyses of FGK stars are made using homogeneous plane-parallel model atmospheres and LTE (local thermodynamic equilibrium) line formation. However, recent abundance analyses using hydrodynamical model atmospheres and non-LTE line formation have demonstrated that the effects of surface inhomogeneities and departures from LTE on abundance analyses are not negligible in the Sun and solar-type stars of different metallicities (e.g., Asplund & García Pérez 2001; Korn et al. 2003; Allende Prieto et al. 2004b; Asplund 2005),

being probably dramatic for very metal-poor stars (Shchukina et al. 2005).

The F8-type star BD +17 4708 has been chosen as a spectrophotometric standard, either primary or secondary, for various systems (e.g., Oke & Gunn 1983; Rufener & Nicolet 1988; Jørgensen 1994; Zhou et al. 2001). In particular, this star is the primary standard of the *Sloan Digital Sky Survey* (SDSS) photometric system (Fukugita et al. 1996; Gunn et al. 1998, 2006; Smith et al. 2002). BD +17 4708 is one of the few stars, and the only subdwarf, with very accurate absolute fluxes (Bohlin & Gilliland 2004b), which allows us to test, in an independent way, the models and different atmospheric parameters that have been derived for it. In particular, it is a unique case in which the effective temperature may be well constrained. Also, it can be quite useful to know, with high accuracy, what the fundamental parameters and overall chemical composition of this star are, given that its model atmosphere and predicted fluxes may be used to complement the observed spectral energy distribution in the transformation of observed magnitudes into physical fluxes in the SDSS.

BD +17 4708 has been studied by several groups (Table 1), who have derived effective temperatures between 5800 K and 6200 K, $[\text{Fe}/\text{H}]$ values between -2.0 and -1.4 and a surface

^{*} Tables 2, 3 and Appendix are only available in electronic form at <http://www.aanda.org>

^{**} Hubble Fellow.

Table 1. Literature data for BD +17 4708. Note that there are two sets of parameters given by Boesgaard et al. (1999): those given in the King (1993, K93) scale, and those given in the Carney (1983a,b, C83) scale. In this table, only values derived for the first time (although mostly taken from the more recent papers) by each author(s) are shown to avoid duplicity.

Reference	T_{eff} (K)	$\log g$	[Fe/H]
Peterson (1981)	5800	4.00	-1.95
Rebolo et al. (1988)	5890	4.00	-1.70
Magain (1989)	5960	3.40	-1.93
Axer et al. (1994)	6100	4.40	-1.42
Spite et al. (1994)	5950	3.30	-1.50
Thévenin & Idiart (1999)	5929	4.02	-1.54
Boesgaard et al. (1999, K93)	6091	3.81	-1.73
Boesgaard et al. (1999, C83)	5956	3.65	-1.81
Fulbright (2000)	6025	4.00	-1.63
Mishenina et al. (2000)	6000	4.00	-1.65
Ryan et al. (2001)	5983	—	-1.86
Simmerer et al. (2004)	5941	3.98	-1.60
Nissen et al. (2004)	5943	3.97	-1.64
Meléndez & Ramírez (2004)	6154	3.93	-1.64
Asplund et al. (2006)	6183	4.11	-1.51

gravity of $\log g \simeq 4.0$ (Fig. 1)¹. In this paper, we present a detailed determination of the atmospheric parameters and the iron abundance of BD +17 4708. A critical comparison with values previously reported in the literature is provided in the Appendix. Due to their relevance for studies of stellar interiors, we also derive the abundances of Mg, Si, and Ca, and discuss the uncertainties in the determination of the oxygen abundance from the 7774 Å triplet, in particular the importance of inelastic collisions with neutral H atoms in the non-LTE computations involved. Our analysis is based on the observed spectral energy distribution and a high resolution, high signal-to-noise (S/N) spectrum of the star.

2. Fitting of the spectral energy distribution

Bohlin & Gilliland (2004b, hereafter BL04b) have measured the spectral energy distribution of BD +17 4708, from the UV (0.17 μm) to the near IR (1.0 μm), with respect to the three primary standards of the *Space Telescope Imaging Spectrograph* (STIS) on the *Hubble Space Telescope* (HST). The accuracy of BL04b measurements is better than 0.5% and therefore, in the absolute scale, their fluxes for BD +17 4708 are as accurate as those of the three white dwarfs used as primary standards. The fluxes measured with STIS for these three white dwarfs have uncertainties that range from 2.5% in the UV to 1% at longer wavelengths, according to BL04b. Thus, the spectral energy distribution of BD +17 4708 is accurate at the level of 2% or even better in some spectral regions.

In Fig. 2, the observed fluxes from BL04b are shown along with theoretical flux distributions computed by R. L. Kurucz² after applying an $E(B - V) = 0.01$ reddening (see Sect. 2.1) according to the Fitzpatrick (1999) parameterization with $R_V = A_V/E(B - V) = 3.1$. The models have $\log g = 3.87$ and $[\text{Fe}/\text{H}] = -1.74$, values that we derive in Sect. 3. The theoretical fluxes have been empirically scaled to the observed one using the

¹ Throughout this paper, we use the standard definitions $[X/Y] = \log(N_X/N_Y) - \log(N_X/N_Y)_\odot$ and $A_X = \log(N_X/N_H) + 12$, where N_X is the number density of the element X. The surface gravity g in $\log g$ is given in cgs units.

² Up-to-date models are available at <http://kurucz.harvard.edu>. The characteristics of the models are explained in Kurucz (1970, 1979).

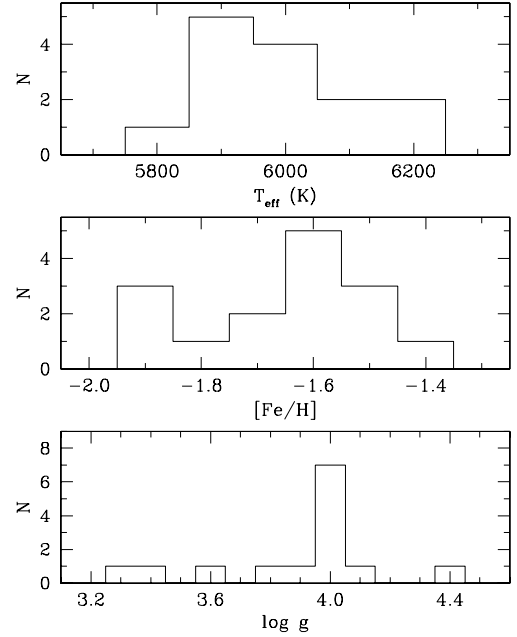


Fig. 1. Distribution of the T_{eff} , $[\text{Fe}/\text{H}]$, and $\log g$ values found in the literature for the star BD +17 4708, as given in Table 1.

reddest 1000 Å, i.e., they were divided by the mean ratio of theoretical to observed fluxes from 9000 Å to 10000 Å in each case. The scaling factor, s , is directly related to the stellar angular diameter, θ , by $s = \theta^2/4$. The spectrum from BL04b was smoothed to approximately match the resolving power of the Kurucz model fluxes.

As shown in Fig. 2, up-to-date Kurucz models, which include newly computed opacity distribution functions, an α -element enhancement consistent with the mean $[\alpha/\text{Fe}]$ ratio we obtain (Sect. 3.7), and without convective overshooting, accurately reproduce (within 1%) the observed flux distribution at wavelengths longer than 5000 Å, as long as the correct $T_{\text{eff}} = 6141$ K is adopted (Sect. 2.2). In the range $4000 \text{ Å} < \lambda < 5000 \text{ Å}$ the model underestimates the flux by about 1.5% while at shorter wavelengths the fit is reasonable on average although several strong lines are not well fitted. Interestingly, a comparison of a MARCS model³ with a Kurucz model of parameters near those of BD +17 4708 (the closest point in the grid we found is: $T_{\text{eff}} = 6000$ K, $\log g = 4.0$, $[\text{Fe}/\text{H}] = -2.0$) shows that the MARCS model predicts fluxes in this region that are larger by about 1%, which would reduce the difference somewhat. Kurucz and MARCS models seem to predict roughly the same fluxes everywhere else.

The Kurucz overshoot model shown in Fig. 2 has the T_{eff} that best fits the data for overshoot models. Clearly, it does not reproduce very well the observational data. The overshoot model does not have α -element enhancement but this has a much smaller effect on the shape of the spectral energy distribution compared to the switch to a no-overshoot model. Note also that the overshoot model that fits best the observations (that shown in Fig. 2) is hotter by about 80 K compared to the no-overshoot model, thus introducing a systematic error in the T_{eff} derived from these fits. For that reason, we prefer to adopt Kurucz no-overshoot models hereafter. Note also that adopting a Kurucz model of $T_{\text{eff}} = 5950$ K, as suggested by previous spectroscopic studies

³ Downloaded from <http://marcs.astro.uu.se>

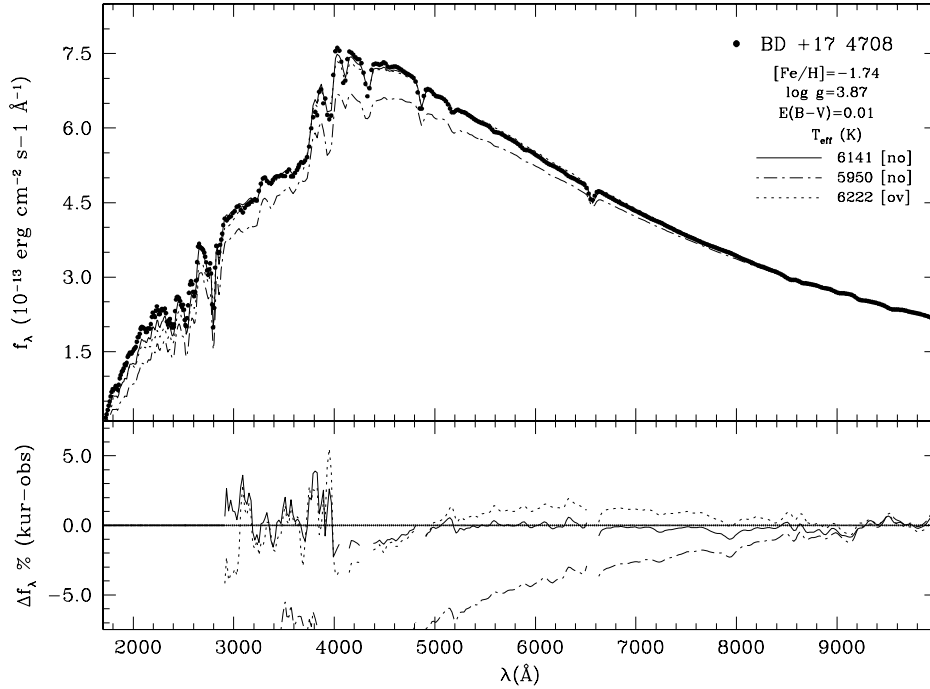


Fig. 2. *Upper panel:* the spectral energy distribution measured by Bohlin & Gilliland (2004b) is shown with the filled circles. Alpha-element enhanced ($[\alpha/\text{Fe}] = +0.4$) no-overshoot [no] Kurucz’s models of $[\text{Fe}/\text{H}] = -1.74$, $\log g = 3.87$, reddened by $E(B - V) = 0.01$ according to the Fitzpatrick (1999) parameterization, and two effective temperatures: $T_{\text{eff}} = 6141 \text{ K}$ and 5950 K , are shown with the solid and dot-dashed lines, respectively. An overshoot [ov] Kurucz model of $T_{\text{eff}} = 6222 \text{ K}$ is shown with the dotted line ($\log g$ and $[\text{Fe}/\text{H}]$ for this model are slightly different to make them consistent with the higher T_{eff}). *Lower panel:* as in the upper panel for the difference (percentile) between observed and theoretical fluxes. The hydrogen lines have been excluded.

(Table 1 and Fig. 1), results in a severe discrepancy with the observational data.

Although it is not shown in Fig. 2, there is a slight degeneracy between T_{eff} and $E(B - V)$ in the model fits to the observed flux distribution. Roughly speaking, increasing T_{eff} is equivalent to decreasing $E(B - V)$, as they both result in higher fluxes in the UV-blue regions while leaving the red and infrared fluxes nearly unchanged (after scaling). For instance, equally good fits to the data can be obtained with $T_{\text{eff}} \approx 6050 \text{ K}$ if no reddening is assumed or with $T_{\text{eff}} \approx 6150 \text{ K}$ if $E(B - V) = 0.010$ is adopted. It is, thus, important to constrain the $E(B - V)$ value independently.

2.1. Reddening

Since BD +17 4708 is at a distance of about 120 pc (its *Hipparcos* parallax is $8.43 \pm 1.42 \text{ mas}$), the $E(B - V)$ value is expected to be negligible or small. The Local Bubble, a region devoid of dense gas extends approximately 60 pc in the direction of BD +17 4708 (Lallement et al. 2003). At the Local Bubble boundary, a significant increase in dense interstellar medium (ISM) material is observed toward several stars in the general direction of BD +17 4708. This ISM material can be observed as narrow absorption lines in high resolution spectra, and depending on the strength of the absorption, it may be expected to cause a small, but measurable, amount of reddening.

Interstellar gas in the line of sight of BD +17 4708 is evidenced by the interstellar Na I D1 ($\sim 5896 \text{ \AA}$) and D2 ($\sim 5890 \text{ \AA}$) lines shown in Fig. 3. Due to the high radial velocity of the star (-291 km s^{-1}), the ISM absorption lines at -13 km s^{-1} are significantly displaced from the strong stellar features. Other than the two stellar lines and two interstellar lines, all of the remaining features seen in Fig. 3 are caused by telluric water vapor.

Although the telluric H_2O lines are relatively weak, they need to be modeled and removed from the spectrum, in order to obtain a high precision measurement of the Na I ISM column density. A relatively simple model of terrestrial atmospheric transmission (AT – Atmospheric Transmission program, from Airhead Software, Boulder, CO) developed by Erich Grossman is used to fit the telluric water vapor lines. This forward modeling technique to remove telluric line contamination in the vicinity of the Na I D lines is described in detail by Lallement et al. (1993), in which a more sophisticated terrestrial atmospheric model was employed. As can be seen in Fig. 3, the AT program is very successful at modeling the terrestrial absorption in the spectrum of BD +17 4708. Note that the stellar lines happen to fall in an area free of contaminating lines, and the two interstellar lines are only slightly blended with water vapor absorption in the wings of the ISM absorption.

The interstellar lines found in the BD +17 4708 spectrum were modeled using standard methods (see, e.g., Sect. 2.2 in Redfield & Linsky 2004a). A single Gaussian absorption component is fit to both Na I D lines simultaneously using atomic data from Morton (2003), and then convolved with the instrumental line spread function. Fitting the lines simultaneously reduces the influence of systematic errors, such as continuum placement and contamination by weak features. The free parameters are the central velocity (v), the line width or Doppler parameter (b), and most importantly, because it can be used to estimate the reddening along the line of sight, the column density (N) of Na I ions toward BD +17 4708. The best fit is shown in Fig. 3, where $v = -13.315 \pm 0.031 \text{ km s}^{-1}$, $b = 3.922 \pm 0.052 \text{ km s}^{-1}$, and $\log N(\text{Na I}) = 11.4776 \pm 0.0034 \text{ cm}^{-2}$. Due to the high S/N, systematic errors probably dominate over the statistical errors given above.

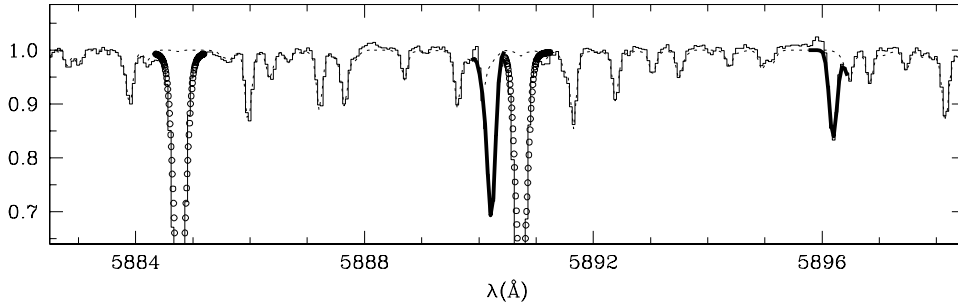


Fig. 3. The observed spectral region around the Na D lines for BD +17 4708, uncorrected for the radial velocity of the star, is shown with the histogram (these observational data are described in Sect. 3.1). The dotted line is the model for telluric water vapor, open circles correspond to the model fit to the stellar lines (see Sect. 3.5), and the thick solid line is the model fit to the interstellar Na D lines (including blends with telluric lines).

The measured line width, a consequence of thermal and non-thermal, or microturbulent, broadening (see Redfield & Linsky 2004b), is wider than typically found for cold ISM clouds (Welty et al. 1994). This is likely due to unresolved interstellar components along the line of sight. Although this observation is considered to be high spectral resolution from a stellar perspective ($\lambda/\delta\lambda \approx 60\,000$, see Sect. 3.1), from an interstellar perspective it is moderate resolution because the narrow and closely spaced component structure typical of the ISM is best observed at much higher resolution ($\lambda/\delta\lambda \approx 500\,000$ – $1\,000\,000$). Therefore, we are likely seeing blending of several ISM components along the line of sight toward BD +17 4708. In fact, π Aqr, a star in the same part of the sky as BD +17 4708 ($\Delta\theta \sim 15^\circ$), but more distant, has been observed at high resolution ($\lambda/\delta\lambda \approx 600\,000$) by Welty et al. (1994). They observed, among 8 total interstellar components, three with velocities between -11 and -13.7 km s $^{-1}$, with a column density weighted average velocity of -12.5 km s $^{-1}$. The total column density for these three components is $\log N(\text{Na I}) = 12.20$ cm $^{-2}$. Because π Aqr is more distant than BD +17 4708, several more components are observed, and a higher column density is to be expected, but the agreement between the two lines of sight, further confirms the interstellar origin of the absorption lines observed in the BD +17 4708 spectrum.

Although we are likely observing several blended ISM components toward BD +17 4708, because the absorption is optically thin, a single component fit to the entire absorption feature should provide a precise measurement of the total Na I column density. It has been shown that, even though most of the ISM Na is ionized, the total Na I column density correlates very well with the total hydrogen column density, $N(\text{H I} + \text{H}_2)$ (Ferlet et al. 1985). Using the relation between $N(\text{Na I})$ and $N(\text{H I} + \text{H}_2)$ provided by Ferlet et al. (1985), which holds for Na I column densities in the range $10.0 \leq \log N(\text{Na I}) \text{ cm}^{-2} \leq 13.0$, we derive a total hydrogen column density of $\log N(\text{H I} + \text{H}_2) = 19.78$ cm $^{-2}$. Bohlin et al. (1978) provide a calibration to transform a total hydrogen column density into an $E(B - V)$ value, which for the highest extinctions has been confirmed by Rachford et al. (2002). Using this relation we obtain a reddening value of $E(B - V) = 0.010$.

No formal error bars are provided for the transformations from $N(\text{Na I})$ to $N(\text{H I} + \text{H}_2)$ or $N(\text{H I} + \text{H}_2)$ to $E(B - V)$. However, we expect the estimate of total hydrogen column density from $N(\text{Na I})$ to be very good because our observed Na I column density is right in the middle of the distribution of points Ferlet et al. (1985) used to calibrate this relation. The transformation from $N(\text{H I} + \text{H}_2)$ to $E(B - V)$ is more difficult because

we are at the lower end of the distribution of measurements used by Bohlin et al. (1978). At these low reddenings, there is some dispersion in the relation due to the low number of discrete absorbers along short sightlines, whereas the relation is significantly tighter for more distant lines of sight, over which a much larger number of ISM environments are averaged. The lowest hydrogen column densities used by Bohlin et al. (1978) are comparable to the column density we observe toward BD +17 4708. Those targets with similar hydrogen column densities have measured reddenings in the range of $E(B - V) = 0.01$ to 0.02 .

Other methods to estimate $E(B - V)$ were also used. The $E(B - V)$ value from the Schuster & Nissen (1989) calibration, which is based on Strömgren photometry, is essentially zero. Interstellar extinction surveys by Fitzgerald (1968) and Arenou et al. (1992) suggest $E(B - V) = 0.000$ and 0.017 , respectively, when used in conjunction with the Hakkila et al. (1997) code, which takes into account the distance to the star. The empirical laws by Bond (1980) and Chen et al. (1998) suggest $E(B - V) = 0.024$ while the integrated extinction maps by Burstein & Heiles (1978) and Schlegel et al. (1998) set upper limits of $E(B - V) = 0.043$ and 0.035 , respectively. Note, however, that all the map estimates have large error bars. A simple mean of the $E(B - V)$ from the maps results in 0.014 ± 0.010 .

Another way to estimate $E(B - V)$ is by means of the use of several homogeneously calibrated unreddened color-temperature relations. In principle, the standard deviation from the mean of several color temperatures minimizes when the appropriate $E(B - V)$ value is used. Thus, we used 14 of the color-temperature relations by Ramírez & Meléndez (2005b) and found the dispersion from the mean T_{eff} to be a minimum with $E(B - V) = 0.008 \pm 0.001$ (see Fig. 4). The real error bar in this $E(B - V)$ value is very likely to be larger due to photometric uncertainties and systematic errors in the T_{eff} -color calibrations. Also, the presence of a cool companion (see Sect. 2.5) may be affecting this estimate by increasing the red and infrared fluxes compared to the case of a single star. In fact, using only blue-visible colors we obtain $E(B - V) = 0.009 \pm 0.002$ (Fig. 4).

In summary, BD +17 4708 is slightly affected by interstellar reddening but the exact $E(B - V)$ is uncertain. Interstellar extinction maps suggest $E(B - V) = 0.014 \pm 0.010$. The $E(B - V)$ value from the T_{eff} -color relations has a more reasonable error of about 0.003 , including systematic errors. If we assume a slightly smaller error to the $E(B - V)$ value from the fit to the ISM lines, e.g., 0.002 , we obtain a weighted mean of $E(B - V) = 0.010 \pm 0.003$. The independent error bars given here are somewhat arbitrary but appropriate for the estimate of the weighted mean.

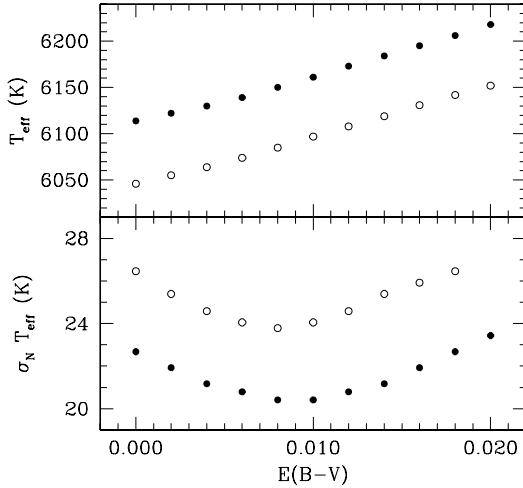


Fig. 4. *Top panel:* mean T_{eff} obtained from the T_{eff} -color calibrations by Ramírez & Meléndez (2005b) as a function of $E(B - V)$ using all colors (14, open circles), and blue-visible colors only (7, filled circles). *Bottom panel:* as in the top panel for the standard error $\sigma_N = \sigma T_{\text{eff}} / \sqrt{N}$, where σ is the standard deviation and N the number of colors used.

2.2. Effective temperature

The BL04b data provides a very reliable way to determine the effective temperature of BD +17 4708 with the help of theoretical flux distributions, provided $\log g$, $[\text{Fe}/\text{H}]$, and $E(B - V)$ are known with sufficient accuracy. In particular, the high sensitivity of the UV continuum flux to T_{eff} can be used to constrain T_{eff} to a level of about 100 K. Even though the completeness of the UV continuum and line opacities in the Kurucz models is controversial (Bell et al. 1994; Balachandran & Bell 1998), the observed UV fluxes have been shown to be reasonably well reproduced by Kurucz models in the Sun (Allende Prieto et al. 2003b), Vega (Bohlin & Gilliland 2004a; García-Gil et al. 2005), and late-type stars of different metallicities (Allende Prieto & Lambert 2000). We did not include the far UV ($\lambda < 2900 \text{ \AA}$) to quantify the quality of the fits in Fig. 2. Not only does this avoid possible errors in the UV fluxes of Kurucz models but it also reduces the impact of errors in the observed flux distribution, which is less accurate at short wavelengths. Nonetheless, including the far UV does not change our conclusions significantly. We also excluded the strong hydrogen lines because they are affected by non-LTE.

As shown in Fig. 2, the UV and blue-visible spectral regions are not well fitted with the $T_{\text{eff}} = 5950 \text{ K}$ model. Any attempt to reconcile the model and observed UV continuum fluxes with an increase in the scaling factor ruins the agreement in the infrared. The best fit to the data is obtained with $T_{\text{eff}} = 6141 \text{ K}$ for $E(B - V) = 0.01$ (see Fig. 5). Given the error in the extinction value derived in Sect. 2.1, the temperature of BD +17 4708 is well constrained, from the flux fit, at the 50 K level, i.e., $T_{\text{eff}} = 6141 \pm 50 \text{ K}$. This 50 K error includes the uncertainties in the other atmospheric parameters ($\log g$, $[\text{Fe}/\text{H}]$) but it is still dominated by the error in the $E(B - V)$ value. A systematic error due to the choice of models is certainly present but not included in the 50 K.

Most previous spectroscopic studies of BD +17 4708 have found a low T_{eff} of about 5950 K (see Table 1 and Fig. 1)⁴. In the Cayrel de Strobel et al. (2001) catalog, for example, the 8 entries

⁴ By “spectroscopic” here we refer to T_{eff} obtained from the excitation and/or ionization balance of iron lines.

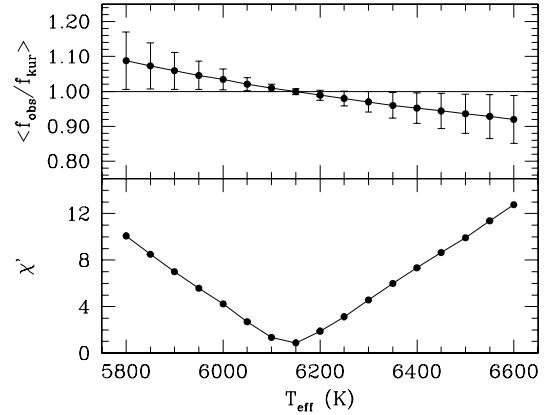


Fig. 5. *Upper panel:* mean value of the ratio of observed (f_{obs}) to scaled theoretical (f_{kur}) fluxes (see Fig. 2) as a function of T_{eff} . *Bottom panel:* the quality of the fit, as given by $\chi^2 = \sqrt{\chi^2/(n-1)}$ where $\chi^2 = \sum_{i=1}^n [(f_{\text{obs}} - f_{\text{kur}})_i^2 / \sigma_i^2]$, as a function of T_{eff} (σ is the error in f_{obs} only).

found for this star have T_{eff} between 5790 K and 6100 K, with the mean T_{eff} being 5960 K. Application of the InfraRed Flux Method (IRFM) for BD +17 4708 resulted in 5955 K according to Ramírez & Meléndez (2005a), who adopted $E(B - V) = 0.000$. Note, however, that if $E(B - V) = 0.010$ is adopted, the IRFM color-temperature calibrations by Ramírez & Meléndez (2005b) suggest $T_{\text{eff}} \approx 6100 \text{ K}$ and if we use blue-visible colors only we obtain $T_{\text{eff}} \approx 6150 \text{ K}$ (Fig. 4). The low temperature obtained from the IRFM and red/infrared photometry is probably due to the presence of a cool companion (see Sect. 2.5). The three highest temperatures in Table 1 are those by Axer et al. (1994), Meléndez & Ramírez (2004), and Asplund et al. (2006). Axer et al. and Asplund et al. derived their T_{eff} from fitting the wings of the Balmer lines, while Meléndez & Ramírez used several IRFM temperature-color relations with a relatively high $E(B - V) \approx 0.02$ value.

2.3. Bolometric flux

The observed absolute flux curve by BL04b covers spectral regions that are difficult to model, namely the UV and blue-visible. Beyond $1.0 \mu\text{m}$, the flux distribution is very well behaved and accurately reproduced by the stellar atmosphere models. Furthermore, the infrared portion of the spectrum is almost insensitive to the choice of effective temperature when the theoretical fluxes are normalized at the Rayleigh-Jeans tail.

The bolometric flux of BD +17 4708 was obtained by integrating the observed flux distribution up to $1.0 \mu\text{m}$ and the predictions from the models for longer wavelengths. Note that for the model fits, as in Fig. 2, the theoretical spectra are the ones that have been reddened. For the bolometric flux calculation, on the other hand, we unreddened the observed flux distribution. Thus, we use the term bolometric flux in the intrinsic sense, i.e., we use it to refer to the flux that would be measured at the top of the Earth’s atmosphere in the absence of interstellar absorption.

The mean error of each point on the observed flux distribution is about 2%. Assuming the error in the models is negligible, our best estimate for the bolometric flux is $f_{\text{bol}} = 4.89 \pm 0.10 \times 10^{-9} \text{ erg cm}^{-2} \text{ s}^{-1}$. This value is in good agreement with that obtained from the Alonso et al. (1995) photometric calibrations for the $(K, V - K)$ pair, which result in $4.80 \times 10^{-9} \text{ erg cm}^{-2} \text{ s}^{-1}$.

2.4. Angular diameter

The angular diameter of BD +17 4708 can be calculated with the f_{bol} and T_{eff} derived above. This value corresponds to the limb-darkened angular diameter. Propagating the 2% error in f_{bol} and 1% error in T_{eff} we determine our best solution for the angular diameter as: $\theta = 0.1016 \pm 0.0023$ mas.

2.5. Binarity

Our model fits (and hence our results for f_{bol} , T_{eff} , etc.) consider BD +17 4708 as a single star. However, it is known that BD +17 4708 shows periodic radial velocity variations with an amplitude of about 4.7 km s^{-1} over a period of about 220 days (Latham et al. 1988). Model fits to the radial velocity curve by Latham et al. suggest a mass function $f(M) = (m_2 \sin i)^3 / (m_1 + m_2)^2 = 0.0019 \pm 0.0004 M_{\odot}$, where m_1 and m_2 are the masses of the stars and i the orbital inclination.

A rough estimate assuming a mass of about $0.9 M_{\odot}$ for the primary (see Sect. 3.5.1), results in a companion mass of $0.15 M_{\odot}$ (using $\langle \sin^3 i \rangle = 3/5$), which corresponds to a late M type star with a $T_{\text{eff}} \sim 3000 \text{ K}$. Using Kurucz model fluxes we find that the contribution of the secondary to the UV and blue fluxes, which are much more sensitive to T_{eff} than the IR, is negligible (less than 1/50). Although the secondary contributes a significant flux in the IR (about 1/5), the *shape* of the spectral energy distribution is nearly unchanged. Given that it is this shape along with a scaling factor what determine the best T_{eff} solution for the primary, including the companion flux in the fits will not affect the T_{eff} result significantly. If included, the scaling factor would need to be reduced and the T_{eff} of the primary increased to match the observed UV and blue fluxes. However, given that the orbital inclination is unknown, it is safer to use a single model flux to fit the observed energy distribution, but note that the companion flux may have an important effect in the observed colors, making them redder. This is probably the reason why direct application of the IRFM suggest a lower T_{eff} for the primary compared to the T_{eff} obtained from the flux fit (Sect. 2.2).

The IRFM temperature of this star is 5950 K according to Ramírez & Meléndez (2005a), who used $E(B - V) = 0$. Using $E(B - V) = 0.01$ the IRFM temperature increases to 6025 K , about 120 K lower than the T_{eff} obtained from the flux fit. It is unlikely that such large difference is due to errors in the absolute infrared flux calibration and/or the zero point determination of the IRFM T_{eff} scale (see Ramírez & Meléndez 2005a for details). The most likely reason for this discrepancy is the flux contributed by the companion, which is more important in the infrared. If the flux at a given wavelength in the infrared (f_{IR}) is larger then the ratio $R = f_{\text{bol}}/f_{\text{IR}}$ is smaller compared to that for a single star. This R -factor is the T_{eff} indicator in the IRFM, roughly proportional to T_{eff}^3 (Ramírez & Meléndez 2005a). Thus, the IRFM temperature obtained for a star with an ignored cool companion is underestimated. In order to account for the 120 K difference (about 2% error in T_{eff}), an error of about 6% in the R -factor is required. In the previous paragraph we estimated a 20% extra infrared flux due to the companion. Using the same models, the bolometric flux increases by about 10% if the cool companion is included. If this is the case, the R -factor has been underestimated by about 8%. However, note again that these flux estimates are not accurate due to the large uncertainty in the mass and temperature of the companion.

3. Spectral line analysis

3.1. Observations

BD +17 4708 was observed from McDonald Observatory on October 30, 2004 UT using the 2dcoudé spectrograph (Tull et al. 1995) and the 2.7 m Harlan J. Smith telescope. Four individual exposures of 20 min each were obtained at the focal station F3 using grating E2 – a 53.67 gr mm^{-1} R2 echelle from Milton Roy Co., a 1.2 arcsec slit, and a 2048×2048 Tektronix CCD. The spectra have a FWHM resolving power of $\lambda/\delta\lambda \simeq 60\,000$ with full spectral coverage from 3600 \AA to 5300 \AA , and substantial but incomplete coverage from 5300 \AA to $10\,000 \text{ \AA}$. The spectra were reduced using the echelle package in IRAF⁵. The bias level in the overscan area was modeled with a polynomial and subtracted. An ultra-high signal-to-noise flatfield was used to correct pixel-to-pixel sensitivity variations, and the scattered light was modeled with smooth functions and removed.

The spectra were optimally extracted after cosmic-ray cleanup, and calibrated in wavelength with a Th-Ar hollow cathode lamp (Allende Prieto 2001). By cross-correlating the four individual spectra, we concluded that shifts among them were smaller than 0.2 km s^{-1} , and we simply coadded their signal obtaining a single spectrum with a signal-to-noise ratio per pixel in excess of 300 between 5000 \AA and 8000 \AA , and in excess of 100 between 4000 \AA and $10\,000 \text{ \AA}$. The individual orders were continuum normalized, combining the signal for the wavelength intervals registered in multiple orders. Similarly to the procedure described by Barklem et al. (2002), we took advantage of the slow variation of the blaze function between orders in the normalization process, in order to derive reliable line shapes for the strongest lines.

3.2. Atomic data

3.2.1. Iron

All the gf values for the iron lines used in this work have been measured in the laboratory. No attempts to reduce the line-to-line scatter in the abundances using differential analysis or astrophysical gf values have been made. Thus, our derived iron abundances are strictly given on an *absolute* scale.

The original sources for the transition probabilities of the Fe I lines are listed by Lambert et al. (1996), who extensively compared them and concluded that they were all essentially on the same scale, although minor corrections are needed in a few cases. The gf values for the Fe II lines have been adopted from Meléndez et al. (2006), who use gf values from theoretical calculations put onto the laboratory scale by means of laboratory lifetimes and branching ratios. Note that these gf -values are very similar to those in Lambert et al. (1996). The mean difference in $\log gf$, in the sense Meléndez et al. (2006) – Lambert et al. (1996), for 4 Fe II lines available in both studies, is only 0.03 dex. A similar comparison with the compilation by Allende Prieto et al. (2002) reveals that, on average, their gf values are on the same scale as those by Meléndez et al. (2006). However, the line-to-line scatter reduces when adopting the latter set of gf values.

Regarding van der Waals pressure broadening, almost all the damping constants adopted in this work are from Barklem et al. (2000) and Barklem & Aspelund-Johansson (2005). For a few

⁵ IRAF is distributed by the National Optical Astronomy Observatories, which are operated by the Association of Universities for Research in Astronomy, Inc., under cooperative agreement with the National Science Foundation – <http://iraf.noao.edu>

Fe I lines not included in the Barklem et al. tables, the classical Unsöld approximation, enhanced by a factor of 2, was adopted. Standard radiative (e.g., Gray 1992) and Stark (e.g., Cowley 1971) broadening approximations, as coded in the latest version of MOOG (Snedden 1973)⁶, were used.

The iron line data and equivalent widths (EW s) measured in the spectrum of BD +17 4708 are given in Table 2, available in electronic form. Gaussian profile fitting was used to measure the line EW s.

3.2.2. Other elements

For the strong 5180 Å Mg I b lines, as well as for the 7774 Å O I triplet, transition probabilities were obtained from the NIST Atomic Spectra Database⁷.

It was difficult to find weak Mg lines with reliable transition probabilities in our spectrum. In fact, we found only the unblended weak 4571 Å Mg I line, with a reliable gf value from the NIST database. Another weak Mg I line is that at 5711 Å, for which we used the solar gf derived by Fuhrmann et al. (1995).

Data for four weak Si I lines were taken from the compilation by Allende Prieto et al. (2004a), who concentrated on lines with transition probabilities measured in the laboratory or obtained from accurate theoretical calculations.

For the Ca abundance determination, we used the line list by Bensby et al. (2003) but adopting the gf values from the NIST database instead of using their solar gf 's. The Bensby et al. gf values are systematically lower by about 0.2 dex compared to those obtained from the NIST database. However, the line-to-line scatter in our derived mean Ca abundance is similar for the two sets of gf values.

Radiative, Stark, and van der Waals broadening was computed in the same way as for the iron lines. Note that in this case all lines are weak (with the exception of the Mg I b triplet and the 6439 Å Ca I line) so the use of the modified Unsöld approximation, when necessary, to obtain the van der Waals damping constants instead of using those from the theory of Barklem et al. (2000) has no noticeable effect on the abundances.

Table 3, available in electronic form, contains the atomic data for the elements described here, as well as the EW s measured in the BD +17 4708 spectrum.

3.3. Modeling

Spectrum synthesis was performed using MOOG (Snedden 1973) and the non-LTE codes TLUSTY and SYNSPEC (Hubeny 1988; Hubeny & Lanz 1995)⁸. For practical reasons, MOOG was preferred for matching the equivalent widths of the iron lines, while SYNSPEC was used to fit the profiles of strong lines. The same scaled solar abundances (those by Grevesse & Sauval 1998) were used in the two codes and thus, only very small differences, mainly due to the continuum opacity calculations, may be present when comparing the results from the two codes. All line formation calculations were done assuming LTE, with the only exception of the 7774 Å triplet (see Sect. 4).

For the line-profile fitting, all the synthetic profiles have been broadened by convolving the theoretical spectra with Gaussian profiles of $FWHM = 0.18$ Å in the red and $FWHM = 0.21$ Å

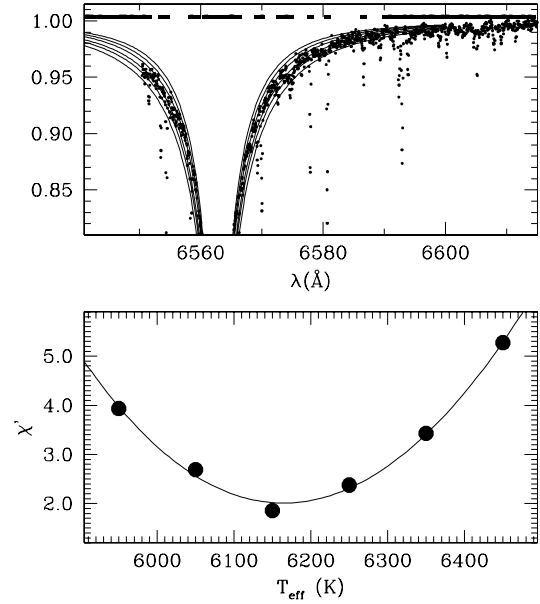


Fig. 6. *Top panel:* the observed $H\alpha$ profile (points) is shown along with model line profiles of $T_{\text{eff}} = 5950, 6050, 6150, 6250, 6350, 6450$ K (solid lines). The bars on top show the regions excluded from the χ^2 calculation. *Bottom panel:* quality of the fits in the top panel, as measured by $\chi' = \sqrt{\chi^2/(n-1)}$ where $\chi^2 = \sum_{i=1}^n [(f_{\text{obs}} - f_{\text{kur}})_i^2 / \sigma_i^2]$ (σ is the error in f_{obs} only), as a function of T_{eff} (filled circles). The solid line is a cubic fit to the filled circles.

in the near infrared. These $FWHM$ values are empirically determined global broadening parameters that fit very well weak lines with reliable atomic data. In fact, given the resolution $R \sim 60\,000$ ($\delta\lambda \sim 0.09$ Å at 5500 Å, $\delta\lambda \sim 0.13$ Å at 7780 Å), a solar-like macroturbulent velocity of 1.5 km s⁻¹ ($\delta\lambda \sim 0.03$ Å at 5500 Å, $\delta\lambda \sim 0.04$ Å at 7780 Å), and a low projected rotational velocity of $v \sin i \sim 3$ km s⁻¹, our estimates for the $FWHM$ values are well justified.

We used the most recent Kurucz no-overshoot model atmospheres with α -element enhancement (e.g., Kurucz 1970, 1979). The use of models with the convective overshooting option switched on produces an almost constant shift of less than 0.1 dex in the abundance scale but preserves abundance ratios as well as the difference in the mean Fe abundances from Fe I and Fe II lines reported in Sect. 3.6. Use of models with solar scaled abundances (i.e., without α -element enhancement) produced essentially the same abundances. For each set of atmospheric parameters adopted, a microturbulent velocity v_t was derived by making the abundances from the Fe I lines independent of their reduced equivalent widths (EW/λ).

3.4. T_{eff} from the Balmer lines

Balmer line-profiles were synthesized using the prescription by Barklem et al. (2002) but adopting Kurucz model atmospheres. In short, Stark broadening was computed according to Stehlé & Hutcheon (1999) while self-broadening is from Barklem et al. (2000). The shapes of strong lines like $H\alpha$ are very well determined in our spectrum by fitting the blaze shape of each clean order (those free from very strong line absorption), and modeling the smooth variation of the shape of the blaze with order number to set the continuum (see Sect. 2 in Barklem et al. 2002 for details).

⁶ <http://verdi.as.utexas.edu/moog.html>

⁷ http://physics.nist.gov/PhysRefData/ASD/lines_form.html

⁸ <http://nova.astro.umd.edu>

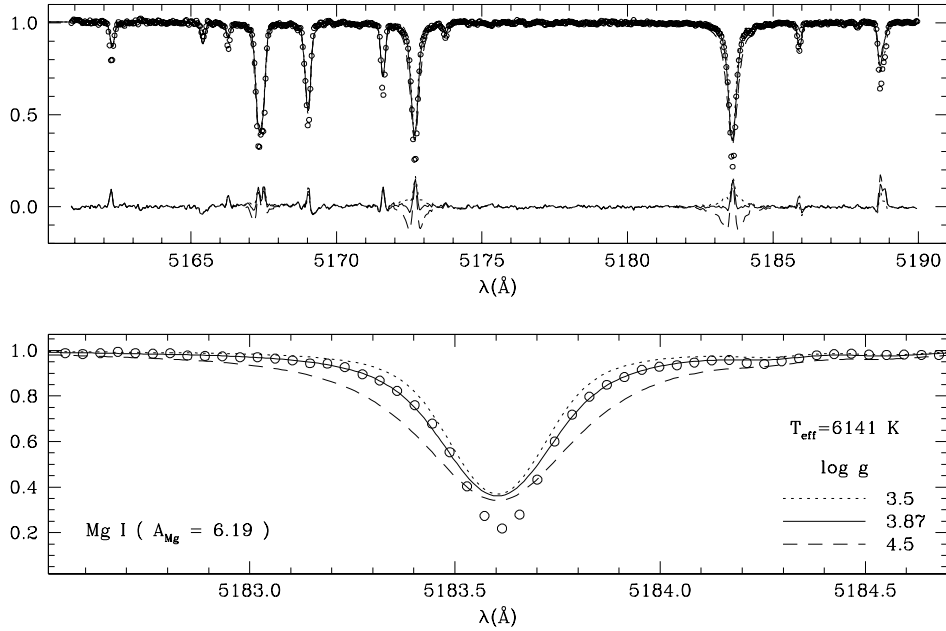


Fig. 7. *Top panel:* the region around the strong Mg I *b* triplet as given by the observations (open circles), and as predicted by models of $T_{\text{eff}} = 6141$ K, $[\text{Fe}/\text{H}] = -1.74$, $A_{\text{Mg}} = 6.19$, and three different values of the surface gravity ($\log g = 3.5, 3.87, 4.5$). Residuals of the fit are also shown. *Bottom panel:* zoom into the 5183.6 Å line.

The results for H α are shown in Fig. 6, along with the observed profile in the spectrum of BD +17 4708. As shown in Fig. 6, the wings of the H α line are very sensitive to T_{eff} . Unfortunately, due to contamination by metallic lines, the H β profile is difficult to use as a temperature indicator.

Excluding the most prominent metallic features, as shown in Fig. 6, a χ^2 test favors a $T_{\text{eff}} = 6165$ K from H α . For the χ^2 calculations, the H α line was cut at 6550 Å since shorter wavelengths fall outside the CCD. In fact, our spectrum in this order goes down to about 6535 Å, but the data points between 6535 Å and 6550 Å are, observationally, somewhat more uncertain. If the blue wing of the H α line is ignored altogether (to minimize further the observational errors), the temperature increases only by 20 K. On the other hand, the sensitivity to T_{eff} decreases for $\lambda > 6590$ Å and, given the S/N, introducing these longer wavelengths to assess the quality of the fits increases only the absolute χ^2 values without changing significantly the inferred T_{eff} .

Our H α temperature is in excellent agreement with that given by Asplund et al. (2006), who obtained $T_{\text{eff}} = 6183$ K from fits to their H α profile using MARCS models but the same treatment for the line broadening. Both, ours and Asplund et al. H α temperatures are in good agreement with the T_{eff} derived from the fitting of the spectral energy distribution.

3.5. Surface gravity from strong lines

The stellar surface gravity of a star can, in principle, be obtained from an estimate of its mass and its measured trigonometric parallax, besides reasonable estimates of T_{eff} and $[\text{Fe}/\text{H}]$. The mass of a nearby star can be reasonably estimated from its position on a color–magnitude diagram using theoretical isochrones but the *Hipparcos* parallax of stars farther than 100 pc, as is the case for BD +17 4708, is quite uncertain and therefore their trigonometric $\log g$ values are not reliable. In fact, using this method we only obtain a weak constrain: $3.8 < \log g < 4.6$.

Fortunately, the wings of some strong lines are sensitive to the $\log g$ value and are less affected by T_{eff} and can thus be used to constrain the surface gravity. In the BD +17 4708 spectrum, only the two strongest lines of the Mg I *b* triplet at 5172.7 Å and 5183.6 Å seem suitable for this kind of analysis (Fig. 7). Note that the cores of the strong lines are strongly affected by non-LTE and we do not expect good fits in the line centers, only the wings should be used to assess the quality of the fits.

Figure 7 shows that an excellent fit to the wings of the Mg I *b* triplet is obtained with $\log g = 3.87$ when the Mg abundance is set to $A_{\text{Mg}} = 6.19$, as derived in Sect. 3.7. Our preferred solution for the surface gravity is thus $\log g = 3.87 \pm 0.08$. The error bar was estimated by propagating the error of 0.06 dex in A_{Mg} , which includes the 50 K error in T_{eff} .

The Mg I *b* triplet is very strong and contaminated by metallic lines in the solar spectrum. Nevertheless, adopting the same procedure we used to obtain the $\log g$ value of BD +17 4708, we were able to satisfactorily reproduce the wings of these lines in the solar spectrum of Kurucz et al. (1984) with the standard solar $\log g = 4.44$ and Mg abundance of $A_{\text{Mg}} = 7.53$ (Asplund et al. 2005). A visual inspection showed that the accuracy of our method of $\log g$ determination in the Sun is about 0.1 dex. Therefore, the $\log g$ value we derive for BD +17 4708 is accurate at the 0.1 dex level in the absolute scale.

3.5.1. Mass, age, and radius from theoretical isochrones

Isochrones in the theoretical HR diagram (T_{eff} vs. $\log g$) instead of the observational HR diagram (absolute magnitude vs. color) can be used to estimate the mass and age of a star if its parameters, but not necessarily its distance, are known with accuracy. This is the case of BD +17 4708.

Although the mass estimates are normally accurate using this approach, the age determinations may be subject to severe systematic errors and statistical biases (see, e.g., Pont & Eyer 2004) so they must not be considered accurate even if the stellar parameters are. We used the Bertelli et al. (2004) isochrones, as

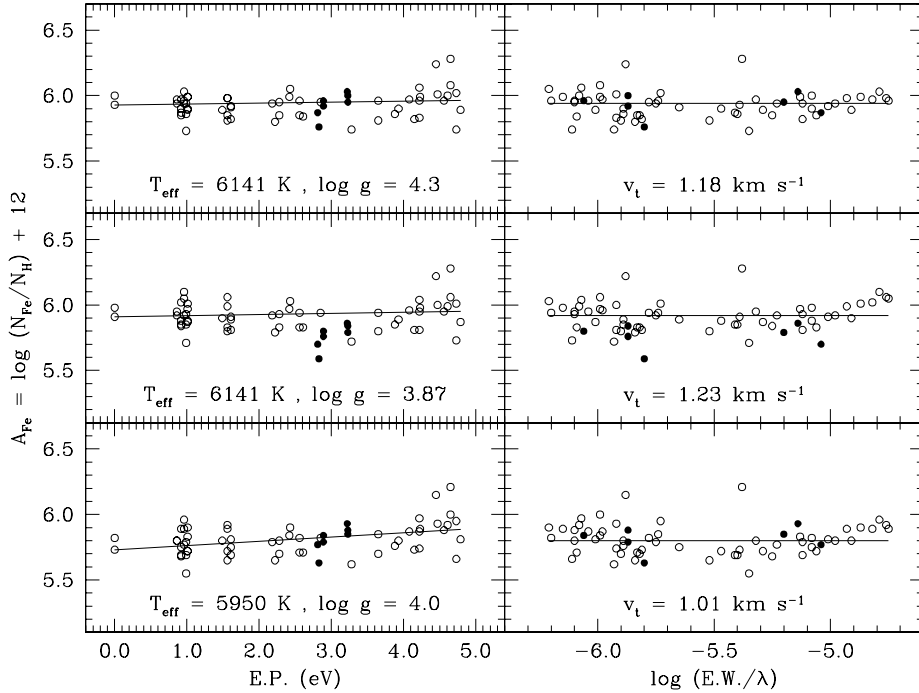


Fig. 8. Abundance of iron from Fe I (open circles) and Fe II lines (filled circles), as determined using different combinations of T_{eff} , $\log g$, and v_t ; as a function of excitation potential and reduced equivalent width. The solid lines are linear fits to the Fe I data only.

in Allende Prieto et al. (2004a), to estimate the mass (M) and age (t) of BD +17 4708. The Bertelli et al. isochrones were computed using solar-scaled chemical compositions. In metal-poor stars, however, the α -element enhancement ($[\alpha/\text{Fe}] \simeq +0.4$ in our case, Sect. 3.7) has an important effect on these calculations (e.g., Vandenberg et al. 2000; Kim et al. 2002) although its effect on the mass and age derived from the isochrones is relatively small (about $+0.1 M_{\odot}$ and -0.4 Gyr in our case). Therefore, we increased the $[\text{Fe}/\text{H}]$ value of BD +17 4708 by about 0.2 dex to mimic the α -element enhancement, as suggested by Salaris et al. (1993) and obtained $M = 0.91^{+0.11}_{-0.04} M_{\odot}$ and $t = 8.8^{+2.6}_{-1.8}$ Gyr (2σ errors).

The referee noted that using our derived parameters the Vandenberg et al. (2000) isochrones suggest an age close to 10 Gyr but if the $\log g$ value is increased to 4.05 then the age would increase to about 13.5 Gyr. Using the Bertelli et al. isochrones and $\log g = 4.05$, we obtained $t = 11.4^{+1.3}_{-4.2}$ Gyr, i.e., an increase of 2.6 Gyr in the mean age. The halo is believed to have an age of about 13 Gyr (e.g., Schuster et al. 2006). However, given that this mean age is calculated using large samples of halo stars and in some cases sophisticated statistics, this should not be used to discard or confirm ages of individual stars. Note that, for example, our derived age is in agreement with that given by Nordström et al. (2004), who took into account the statistical biases in isochrone age determinations described in Pont & Eyer (2004). Also, some halo stars, even more metal-poor than BD +17 4708, seem to be younger than the mean age of the halo (see, e.g., Table 2 in Li & Zhao 2004, who give a compilation of radioactive ages, including theirs).

The radius that we obtain using isochrones is about $1.8 R_{\odot}$, with a $2\text{-}\sigma$ range that goes from 1.5 to $2.3 R_{\odot}$ if we include systematic errors in our T_{eff} and $\log g$ estimates. Although inaccurate, the *Hipparcos* parallax constrains the radius to a $1\text{-}\sigma$ range from 1.1 to $1.6 R_{\odot}$, if we adopt our angular diameter (Sect. 2.4). A slightly higher $\log g$ value, for example $\log g = 4.0$, would result in $R \simeq 1.4 R_{\odot}$. Note that this would still be in good,

albeit marginal, agreement with our result for $\log g$ considering the random error bar (0.08 dex) and a possible systematic error in the absolute scale (about 0.10 dex).

3.6. The iron abundance

The customary approach to a determination of the Fe abundance invokes LTE for the excitation and ionization of iron neutral atoms and singly-charged ions. An estimate of the effective temperature is obtained by the requirement that the derived Fe abundances from the Fe I lines be independent of their excitation potential. Application of this requirement generally demands a prior determination of the microturbulence (v_t), often from the same set of Fe I lines and the condition that the Fe abundance be independent of a line's EW . Then, the imposition of ionization equilibrium through the requirement that the Fe I and Fe II lines give the same Fe abundance defines a locus in the $(T_{\text{eff}}, \log g)$ plane which with the T_{eff} from the Fe I lines (or another source) serves to determine the surface gravity.

We used 56 Fe I lines covering the excitation potential (EP) range from 0 to 5 eV and 7 Fe II lines to derive the iron abundance for various choices of atmospheric parameters (Figs. 8 and 9). The lines we selected have EW between 4 and $100 \text{ m}\text{\AA}$ to avoid errors due to noise and saturation.

The Fe I lines with an almost 5 eV range in excitation potential demand an effective temperature only slightly larger than about 6141 K (Fig. 8), almost independently of the choice of surface gravity, and confirming the temperature provided by the flux distribution. A temperature of 5950 K is demonstrably too low.

A correlation between the excitation potential of the lines and their reduced equivalent widths may lead to degenerate solutions for the (T_{eff}, v_t) pair. There is no such correlation for our Fe I lines with $EP > 2$ eV. Our Fe I lines with $EP < 2$ eV do not show such correlation either but they are all stronger (i.e., they all have larger reduced equivalent widths) than those with

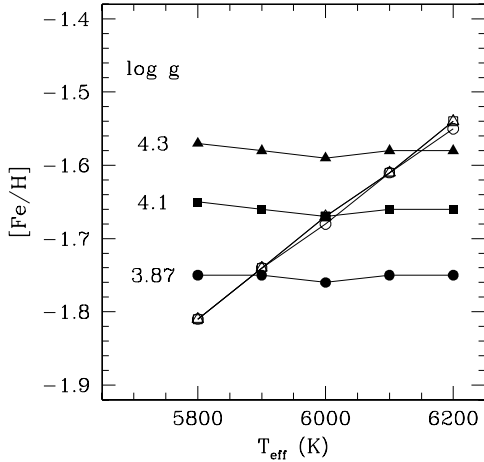


Fig. 9. Mean abundance of iron from Fe I (open symbols) and Fe II (filled symbols) lines as a function of T_{eff} and $\log g$. Here $[\text{Fe}/\text{H}] = A_{\text{Fe}} - 7.51$, i.e., we used $A_{\text{Fe}} = 7.51$ for the Sun.

EP > 2 eV. The strong, low EP lines allow to better determine ν_i . Notice, however, that the A_{Fe} vs. EP relations shown in Fig. 8 do not change dramatically if the lowest EP lines are avoided.

The LTE ionization equilibrium is satisfied at the locus shown in Fig. 10. At $T_{\text{eff}} = 6141$ K, the locus (see also Fig. 9) corresponds to about $\log g = 4.3$, a value higher than that provided by the fit to the Mg I *b* lines. Note that this result is inconsistent with that found by Edvardsson (1988), who concludes that the strong line gravities are larger than those obtained from the ionization balance in a sample of subgiants with metallicities higher than about $[\text{Fe}/\text{H}] = -0.5$. At that lower value of $\log g = 3.87$ and $T_{\text{eff}} = 6141$ K, the Fe abundance from Fe II lines is about 0.15 dex less than that from the Fe I lines, as it is clearly seen in the middle panels of Fig. 8. Ionization equilibrium at $\log g = 3.87$ is achieved if $T_{\text{eff}} \approx 5900$ K, but this temperature is judged to be too low.

Our analysis shows that a consistent analysis of the flux distribution and the Mg I *b*, Fe I, and Fe II lines cannot be found within the constraints of a classical LTE model atmosphere analysis. The inconsistencies, almost certainly, cannot be ascribed to the accumulation of errors in the flux and line data. One must suspect a failure of the classical atmosphere and/or the breakdown of the LTE assumption.

Introduction of departures from LTE into the formation of iron lines within a classical model atmosphere constructed assuming LTE for all sources of continuous and line opacity calls for atomic data on radiative and collisional processes far beyond the restricted need for the corresponding LTE analysis. The main non-LTE effect on the Fe lines has been shown to be an overionization of neutral Fe atoms resulting from the UV flux (e.g., Athay & Lites 1972). This effect is the more severe for metal-poor stars owing, principally, to the reduced line blocking in the UV.

Calculations reported for HD 140283, a star more metal-poor and cooler than BD +17 4708, show that, using 1D model atmospheres (see next paragraph), the Fe abundance from the Fe I lines might be increased by up to about 0.5 dex for a non-LTE analysis (e.g., Korn et al. 2003; Shchukina et al. 2005) while leaving the Fe abundance from the Fe II lines nearly unchanged. If these non-LTE effects are taken into account in our case, they would increase further the difference between the Fe abundance from the neutral and ionized lines and would require even higher surface gravities to achieve ionization equilibrium. Note,

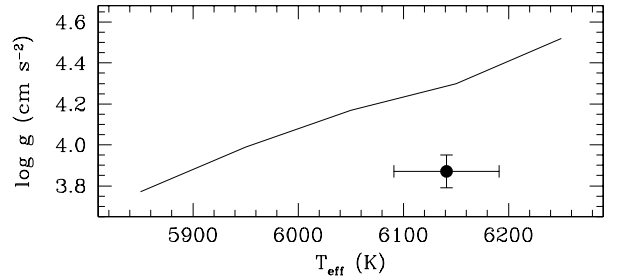


Fig. 10. Locus of the T_{eff} and $\log g$ values for which ionization equilibrium of Fe lines is satisfied. The circle with the error bars correspond to our best estimates of T_{eff} from the flux distribution and $\log g$ from the fit of the Mg I *b* lines.

however, that the role of inelastic collisions with neutral hydrogen in the non-LTE calculations needs to be explored in more detail given that they may significantly reduce the size of the non-LTE corrections to the Fe I abundance (Korn et al. 2003). In fact, we find that they are very important for the oxygen abundance determination from the 7774 Å triplet although the formulation commonly adopted (that by Steenbock & Holweger 1984) is questionable and the resulting abundances uncertain (see Sect. 4).

Classical atmospheres with their assumption of plane parallel homogeneous layers in hydrostatic equilibrium cannot represent the stellar granulation resulting from convective instabilities. Modeling of granulation in main-sequence stars including metal-poor examples is beginning with attendant analyses of LTE and non-LTE line formation (Asplund 2005). The latter models are commonly referred to as 3D models with classical models as 1D models. Calculations for HD 140283 suggest that the non-LTE Fe abundance from the Fe II lines is increased by about 0.3 dex in going from a 1D to a 3D model of the same atmospheric parameters but the non-LTE abundance from Fe I lines is unchanged (Shchukina et al. 2005).

Taking the results for HD 140283 at face value, and applying them to our case, the switch from the 1D LTE analysis to the 3D non-LTE one (without H collisions) would lead to an increase of about +0.2 dex in the Fe I – Fe II abundance difference (the Fe I abundance increasing by 0.5 dex due to non-LTE in 1D and the Fe II abundance increasing by 0.3 dex due to 3D effects in non-LTE). Thus, if the sense and approximate magnitude of these effects applies to BD +17 4708, the disagreement between the surface gravity derived from the LTE analysis of the Mg I *b* lines and Fe ionization equilibrium is increased. Excitation by collisions with H atoms could alleviate the disagreement discussed somewhat but no reliable theory to include them in the non-LTE calculations is available at present (see Sect. 4).

There is clearly a need for a fuller exploration of the non-LTE effects (in particular H collisions) both in the construction of the model atmosphere and in the line formation. Detailed testing of 3D models is a necessity with confrontation between predictions of the energy distribution, line strengths, wavelengths, and asymmetries. Pending this major challenge, we conclude that the best fits to the data so far have been achieved with $T_{\text{eff}} = 6141$ K and $\log g = 3.87$. Given that the Fe II lines seem to be less affected by errors in T_{eff} or non-LTE (see, e.g., Thévenin & Idiart 1999; but see also Shchukina et al. 2005), we disregard the ionization balance condition and adopt the mean abundance from the Fe II lines only as our $[\text{Fe}/\text{H}]$ indicator. Thus, our preferred solution for the metallicity of BD +17 4708 is

$[\text{Fe}/\text{H}] = -1.74 \pm 0.09$, which, for our inferred solar iron abundance⁹, corresponds to $A_{\text{Fe}} = 5.77 \pm 0.09$ ¹⁰.

3.7. Mg, Si, and Ca abundances

Besides their importance in the study of Galactic chemical evolution, the abundances of these elements are relevant for stellar structure and evolution calculations (e.g., VandenBerg et al. 2000). Although they are less abundant than carbon, nitrogen, and oxygen, they are important sources of opacity at high temperatures.

It is well established that the $[\alpha/\text{Fe}]$ ratios, where α is an α element (e.g., Mg, Si, Ca, etc.), in the majority of metal-poor stars are well above solar. Most authors agree on $[\alpha/\text{Fe}]$ ratios of about $+0.3 \pm 0.1$ dex in the halo (e.g., Carretta et al. 2000; Gratton et al. 2000; Idiart & Thévenin 2000; Arnone et al. 2005; Barklem et al. 2005).

The Mg abundance was obtained by averaging the abundance derived from the 4571 Å and 5711 Å lines. However, due to the more reliable transition probability of the former, we gave a double weight to the Mg abundance obtained from the 4571 Å line. In this way we find $A_{\text{Mg}} = 6.19 \pm 0.05$. The four Si lines listed in Table 3 resulted in $A_{\text{Si}} = 6.12 \pm 0.06$ while the Ca lines suggest $A_{\text{Ca}} = 4.93 \pm 0.06$.

Almost all the Mg, Si, and Ca lines used to derive the abundances given above are very strong ($EW \gg 90$ mÅ) in the solar spectrum, which makes them unsuitable to derive solar abundances due to saturation effects. Instead, we used the solar abundances derived by Asplund et al. (2005) to obtain $[\text{Mg}/\text{Fe}] = 0.40 \pm 0.10$, $[\text{Si}/\text{Fe}] = 0.35 \pm 0.11$, and $[\text{Ca}/\text{Fe}] = 0.36 \pm 0.11$, where the error due to the uncertainties in $[\text{Fe}/\text{H}]$ and T_{eff} have been included. The mean $[\alpha/\text{Fe}]$ ratio is 0.37 ± 0.06 , where the error bar here is a standard error.

4. The O I triplet: non-LTE effects and $[\text{O}/\text{Fe}]$ ratio

The observed oxygen abundances are relevant for studies of chemical evolution of the Galaxy and supernovae yields (e.g., Wheeler et al. 1989), as well as for the modeling of stellar structure and evolution (e.g., VandenBerg & Stetson 1991).

The IR triplet lines are strong enough as to be detected in most metal-poor FGK dwarfs and it has been long known that they suffer from strong departures from LTE (e.g., Eriksson & Toft 1979; Kiselman 1993; Shchukina et al. 2005). Accurate oxygen model atoms are available in the literature (e.g., Allende Prieto et al. 2003a; Shchukina et al. 2005), which allow to confidently perform non-LTE calculations. The importance of inelastic collisions with neutral H, often neglected in the non-LTE calculations, have been explored by Allende Prieto et al. (2004b) and shown to be necessary to accurately reproduce the center-to-limb variation of the triplet line-profiles in the solar spectrum. Studies of the O I triplet are also important because the triplet lines are excellent probes of the physics of line formation (e.g., Reetz 1999).

⁹ Our line list and adopted atomic data result in $A_{\text{Fe},\odot} = 7.51 \pm 0.08$, with no significant difference between the Fe I and Fe II abundances, although not all the lines could be used in the solar spectrum due to saturation. Details will be given in Ramírez et al. (2006).

¹⁰ Unless otherwise noted, all the error bars for the abundances are $1-\sigma$ errors.

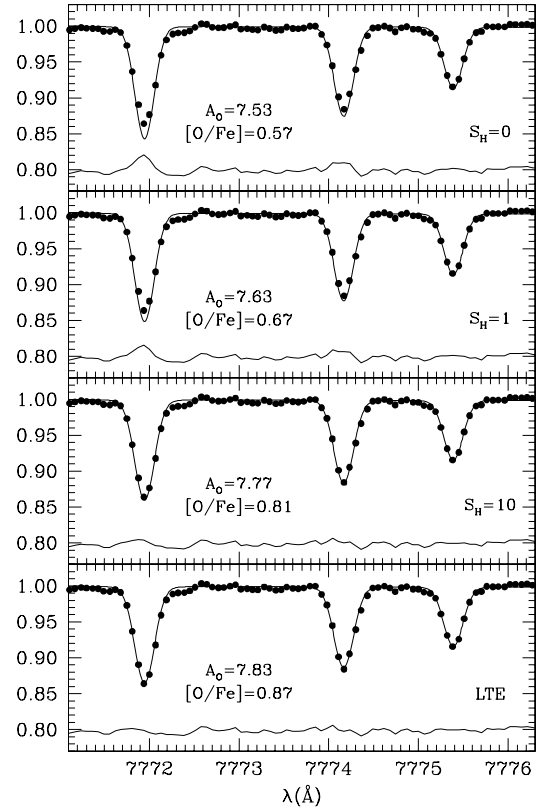


Fig. 11. Observed profile of the O I triplet in BD +17 4708 (filled circles). Non-LTE model fits to the data (solid lines) are shown for $S_{\text{H}} = 0, 1$, and 10 . LTE fits are also shown. The abundances adopted in each case, given in each panel, have been chosen to fit the reddest line of the triplet. Residuals, shifted by $+0.80$, are shown at the bottom of each panel.

Using the exact same atomic model and non-LTE calculations as those used in Allende Prieto et al. (2004b)¹¹, we computed non-LTE line-profiles and compared them to those observed in the spectra of BD +17 4708 (Fig. 11). LTE profiles were also computed for completeness. Non-LTE calculations were made both with and without including H collisions. In the former case, the simple approximation formula by Drawin (1968), enhanced by an empirical factor S_{H} , as suggested by Steenbock & Holweger (1984), was adopted.

The effect of including H collisions is evident from the fits in Fig. 11. Our non-LTE calculations without H collisions, when forced to fit the reddest line of the triplet by tuning the oxygen abundance, overestimate the two strongest lines of the triplet. As S_{H} is increased, the three lines are better fitted, simultaneously, while reducing the size of the non-LTE correction to the oxygen abundance at the same time. A very good fit to the BD +17 4708 triplet profile is found with $S_{\text{H}} = 10$. Note, however, that in the solar case the $S_{\text{H}} = 1$ model fits accurately the center-to-limb observations (Allende Prieto et al. 2004b). Although Allende Prieto et al. did not test non-LTE calculations with $S_{\text{H}} = 10$, such case would lead to an oxygen abundance in disagreement with the other oxygen abundance indicators.

The triplet lines originate from the $3s^2S^0$ to $3p^2P$ transition. The upper level consists of three states with very similar energies but noticeably different transition probabilities. This

¹¹ Allende Prieto et al. used both 1D and 3D model atmospheres in their study. We remind the reader that our work is restricted to 1D Kurucz models.

implies that the depths of formation of the three lines are different. The bluest, strongest line is formed in an upper layer while the reddest, weakest line of the triplet is formed in a deeper layer. Since the density of neutral hydrogen decreases with depth in the stellar atmosphere, the collisional rates due to neutral H are more important in the upper layers thus thermalizing more efficiently the $3p^5P$ levels, which results in a weakening of the line strengths. Considering the different formation depths of the three lines and the fact that the $3p^5P$ level becomes progressively more thermalized with height due to H-collisions, the bluest line of the triplet gets more weakened than the reddest line. This reasoning is consistent with what is shown in Fig. 11.

Adopting $A_O = 8.70$ for the Sun, we find an LTE $[O/Fe]$ ratio of 0.87 for BD +17 4708. The best non-LTE fit to the data, that for $S_H = 10$, reduce this ratio to 0.81. Oxygen abundances in metal-poor stars have been determined by several groups using different lines and types of analyses without general agreement. The so-called “oxygen abundance problem” is complex and still open (see, e.g., Nissen et al. 2002; Fulbright & Johnson 2003; Meléndez et al. 2006). Discrepancies regarding whether the $[O/Fe]$ ratios remain constant at about +0.5 for the most metal-poor stars or if they increase as lower $[Fe/H]$ values are reached still exist although most authors favor constant $[O/Fe]$ ratios. In view of our results for BD +17 4708, we conclude that H-collisions are an important ingredient in the non-LTE computations of the triplet, not to be ignored in metal-poor stars. However, it is still unclear if the approximation adopted in this work is accurate, given that two different values of S_H are needed to fit the spectra of the Sun and a metal-poor star. In any case, when non-LTE oxygen abundances are inferred from the triplet, the three observed line profiles must be accurately reproduced, simultaneously, by the models. At present, our analysis does not allow us to give a reliable estimate of the oxygen abundance of BD +17 4708.

5. Conclusions

The high accuracy with which the spectral energy distribution of the SDSS standard BD +17 4708 has been measured has allowed us to provide a reliable estimate of its effective temperature. We have then used spectral line analysis to infer consistent parameters for this star.

Once the degeneracy between T_{eff} and $E(B - V)$ in the model fits to the observed flux distribution is broken by independent estimates of $E(B - V)$, which included a detailed modeling of interstellar absorption features in the observed spectrum, we obtain the following parameters, given here along with reasonable estimates of the (1σ) error bars: $T_{\text{eff}} = 6141 \pm 50$ K, $[Fe/H] = -1.74 \pm 0.09$, $\log g = 3.87 \pm 0.08$, $E(B - V) = 0.010 \pm 0.003$. The spectral energy distribution also allowed us to obtain reliable values for the bolometric flux, $f_{\text{bol}} = 4.89 \pm 0.10 \times 10^{-9}$ erg cm $^{-2}$ s $^{-1}$, and angular diameter, $\theta = 0.1016 \pm 0.0023$ mas, of the star. We thus provide accurate (in an absolute sense) parameters for the spectrophotometric standard of the *Sloan Digital Sky Survey*.

Compared to previous spectroscopic studies, our T_{eff} is higher by about 190 K, which has a severe impact on classical abundance analyses of moderately metal-poor stars. For example, this increase ruins the good agreement between the iron abundance derived from Fe I and Fe II lines found when a lower T_{eff} is used. Despite this, all other features on the spectrum (e.g., the Balmer lines or the strong Mg lines used to constrain the $\log g$ value) seem to be more consistent with the models when a high T_{eff} is adopted. In particular, the excitation

balance of Fe I lines is satisfied with the high T_{eff} but not with the lower value.

We also determine the mean abundance of α -elements ($[\alpha/Fe] = 0.37 \pm 0.06$). The non-LTE modeling of the permitted oxygen triplet lines should include the effect of collisions with neutral H to reasonably reproduce the observations but a better physical treatment of H collisions is needed.

Acknowledgements. This work was supported in part by the Robert A. Welch Foundation of Houston, Texas. CAP research is funded by NASA (NAG5-13057 and NAG5-13147). S.R. would like to acknowledge support provided by NASA through Hubble Fellowship grant HF-01190.01-A awarded by the Space Telescope Science Institute, which is operated by the Association of Universities for Research in Astronomy, Inc., for NASA, under contract NAS5-26555. We thank Jorge Meléndez for useful advice on interstellar reddening from maps, Martin Asplund for sending us a MARCS model atmosphere, and the referee, Andreas Korn, for comments and suggestions that helped improve the paper.

References

- Allende Prieto, C. 2001, The Spectrum of the Th-Ar Hollow-Cathode Lamp Used with the 2dcoude Spectrograph, McDonald Observatory Technical Note [arXiv:astro-ph/0111172], <http://hebe.as.utexas.edu/2dcoude/thar/>
- Allende Prieto, C., & Lambert, D. L. 2000, AJ, 119, 2445
- Allende Prieto, C., Asplund, M., García López, R. J., & Lambert, D. L. 2002, ApJ, 567, 544
- Allende Prieto, C., Lambert, D. L., Hubeny, I., & Lanz, T. 2003a, ApJ, 147, 363
- Allende Prieto, C., Hubeny, I., & Lambert, D. L. 2003b, ApJ, 591, 1192
- Allende Prieto, C., Barklem, P. S., Lambert, D. L., & Cunha, K. 2004a, A&A, 420, 183
- Allende Prieto, C., Asplund, M., & Fabiani Bendicho, P. 2004b, A&A, 423, 1109
- Alonso, A., Arribas, S., & Martínez-Roger, C. 1995, A&A, 297, 197
- Alonso, A., Arribas, S., & Martínez-Roger, C. 1996, A&AS, 117, 227
- Arenou, F., Grenon, M., & Gomez, A. 1992, A&A, 258, 104
- Arnone, E., Ryan, S. G., Argast, D., et al. 2005, A&A, 430, 507
- Asplund, M. 2005, ARA&A, 43, 481
- Asplund, M., & García Pérez, A. E. 2001, A&A, 372, 601
- Asplund, M., Grevesse, N., & Sauval, A. J. 2005, in Cosmic Abundances as Records of Stellar Evolution and Nucleosynthesis, ed. T. G. Barnes, & F. Bash (San Francisco, ASP), ASP Conf. Ser., 336, 25
- Asplund, M., Lambert, D. L., Nissen, P. E., et al. 2006, ApJ, 644, 229
- Athay, R. G., & Lites, B. W. 1972, ApJ, 176, 809
- Axer, M., Fuhrmann, K., & Gehren, T. 1994, A&A, 291, 895
- Balachandran, S. C., & Bell, R. A. 1998, Nature, 392, 791
- Barklem, P. S., & Asplund-Johansson, J. 2005, A&A, 435, 373
- Barklem, P. S., Piskunov, N., & O’Mara, B. J. 2000, A&AS, 142, 467
- Barklem, P. S., Stempels, H. C., Allende Prieto, C., et al. 2002, A&A, 385, 951
- Barklem, P. S., Christlieb, N., Beers, T. C., et al. 2005, A&A, 439, 129
- Bell, R. A., Paltoglou, G., & Tripicco, M. J. 1994, MNRAS, 268, 771
- Bensby, T., Feltzing, S., & Lundström, I. 2003, A&A, 410, 527
- Bertelli, G., Bressan, A., Chiosi, C., et al. 1994, A&AS, 106, 275
- Biémont, E., Baudoux, M., Kurucz, R. L., et al. 1991, A&A, 439, 539
- Boesgaard, A. M., King, J. R., Deliyannis, C., & Vogt, S. S. 1999, AJ, 117, 492
- Bohlin, R. C., & Gilliland, R. L. 2004a, AJ, 127, 3508
- Bohlin, R. C., & Gilliland, R. L. 2004b, AJ, 128, 3053 (BL04b)
- Bohlin, R. C., Savage, B. D., & Drake, J. F. 1978, ApJ, 224, 132
- Bond, H. E. 1980, ApJS, 44, 517
- Burstein, D., & Heiles, C. 1978, ApJ, 225, 40
- Carney, B. W. 1983a, AJ, 88, 610 (C83)
- Carney, B. W. 1983b, AJ, 88, 623 (C83)
- Carretta, E., Gratton, R. G., & Sneden, C. 2000, A&A, 356, 238
- Cayrel de Strobel, G., Soubiran, C., & Ralite, N. 2001, A&A, 373, 159
- Chen, B., Vergely, J. L., Valette, B., & Carraro, G. 1998, A&A, 336, 137
- Cowley, C. R. 1971, The Observatory, 91, 139
- Drawin, H. W. 1968, Z. Phys., 211, 404
- Edvardsson, B. 1988, A&A, 190, 148
- Eriksson, K., & Toft, S. C. 1979, A&A, 71, 178
- Ferlet, R., Vidal-Madjar, A., & Gry, C. 1985, ApJ, 298, 838
- Fitzgerald, M. P. 1968, AJ, 73, 983
- Fitzpatrick, E. L. 1999, PASP, 111, 63
- Fuhrmann, K., Axer, M., & Gehren, T. 1995, A&A, 301, 492
- Fulbright, J. P. 2000, AJ, 120, 1841
- Fulbright, J. P., & Johnson, J. A. 2003, ApJ, 595, 1154

- Fukugita, M., Ichikawa, T., Gunn, J. E., et al. 1996, *AJ*, 111, 1748
- García-Gil, A., García-Lopez, R. J., Allende Prieto, C., & Hubeny, I. 2005, *ApJ*, 623, 460
- Gratton, R. G., Carretta, E., Matteucci, F., & Sneden, C. 2000, *A&A*, 358, 671
- Gray, D. 1992, *The observation and analysis of stellar photospheres*, 2nd ed. (Cambridge University Press), 207
- Grevesse, N., & Sauval, A. J. 1998, *Space Sci. Rev.*, 85, 161
- Gunn, J. E., Carr, M., Rockosi, C., et al. 1998, *AJ*, 116, 3040
- Gunn, J. E., Siegmund, W. A., Mannery, E. J., et al. 2006, *AJ*, 131, 2332
- Hakkila, J., Myers, J. M., Stidham, B. J., & Hartmann, D. H. 1997, *AJ*, 114, 2043
- Hubeny, I. 1988, *Computer Phys. Comm.*, 52, 103
- Hubeny, I., & Lanz, T. 1995, *ApJ*, 439, 875
- Idiart, T., & Thévenin, F. 2000, *ApJ*, 541, 207
- Jørgensen, I. 1994, *PASP*, 106, 967
- Kim, Y. C., Demarque, P., Yi, S. K., & Alexander, D. R. 2002, *ApJS*, 143, 499
- King, J. R. 1993, *AJ*, 106, 1206 (K93)
- Kiselman, D. 1993, *A&A*, 275, 269
- Korn, A. J., Shi, J., & Gehren, T. 2003, *A&A*, 407, 691
- Kurucz, R. L. 1970, *SAO Special Report*, No. 308
- Kurucz, R. L. 1979, *ApJS*, 40, 1
- Kurucz, R. L., Furenlid, I., Brault, J., & Testerman, L. 1984, *NSO Atlas No. 1: Solar Flux Atlas from 296 to 1300 nm, Sunspot*, NSO
- Lallement, R., Bertin, P., Chassefière, & Scott, N. 1993, *A&A*, 271, 734
- Lallement, R., Welsh, B. Y., Vergely, J. L., et al. 2003, *A&A*, 441, 447
- Lambert, D. L., Heath, J. E., Lemke, M., & Drake, J. 1996, *ApJS*, 103, 183
- Latham, D. W., Mazeh, T., Carney, B. W., et al. 1988, *AJ*, 96, 567
- Li, J., & Zhao, G. 2004, *ChJAA*, 4, 75
- Magain, P. 1987, *A&A*, 181, 323
- Magain, P. 1989, *A&A*, 209, 211
- Meléndez, J., & Ramírez, I. 2004, *ApJ*, 615, L33
- Meléndez, J., Shchukina, N. G., Vasiljeva, I. E., & Ramírez, I. 2006, *ApJ*, 642, 1082
- Mishenina, T. V., Korotin, S. A., Klochkova, V. G., & Panchuk, V. E. 2000, *A&A*, 353, 978
- Morton, D. C. 2003, *ApJS*, 149, 205
- Nissen, P. E., Primas, F., Asplund, M., & Lambert, D. L. 2002, *A&A*, 390, 235
- Nissen, P. E., Chen, Y. Q., Asplund, M., & Pettini, M. 2004, *A&A*, 415, 993
- Nordström, B., Mayor, M., Andersen, J., et al. 2004, *A&A*, 418, 989
- O'Brian, T. R., Wickliffe, M. E., Lawler, J. E., et al. 1991, *J. Opt. Soc. Am.*, B8, 1185
- Oke, J. B., & Gunn, J. E. 1983, *ApJ*, 266, 713
- Peterson, R. C. 1981, *ApJ*, 244, 989
- Pont, F., & Eyer, L. 2004, *MNRAS*, 351, 487
- Rachford, B. L., Snow, T. P., Tumlinson, J., et al. 2002, *ApJ*, 577, 221
- Ramírez, I., & Meléndez, J. 2005a, *ApJ*, 626, 446
- Ramírez, I., & Meléndez, J. 2005b, *ApJ*, 626, 465
- Ramírez, I., Allende Prieto, C., & Lambert, D. L. 2006, in preparation
- Rebolo, R., Beckman, J. E., & Molaro, P. 1988, *A&A*, 192, 192
- Redfield, S., & Linsky, J. L. 2004a, *ApJ*, 602, 776
- Redfield, S., & Linsky, J. L. 2004b, *ApJ*, 613, 1004
- Reetz, J. 1999, Ph.D. Thesis, Ludwig-Maximilians Univ.
- Rufener, F., & Nicolet, B. 1988, *A&A*, 206, 357
- Ryan, S. G., Norris, J. E., & Beers, T. C. 1999, *ApJ*, 523, 654
- Ryan, S. G., Kajino, T., Beers, T. C., et al. 2001, *ApJ*, 549, 55
- Salaris, M., Chieffi, A., & Straniero, O. 1993, *ApJ*, 414, 580
- Schlegel, D. J., Finkbeiner, D. P., & Davis, M. 1998, *ApJ*, 500, 525
- Schuster, W. J., & Nissen, P. E. 1989, *A&A*, 221, 65
- Shchukina, N. G., Trujillo Bueno, J., & Asplund, M. 2005, *ApJ*, 618, 939
- Simmerer, J., Sneden, C., Cowan, J. J., et al. 2004, *ApJ*, 617, 1091
- Smith, J. A., Tucker, D. L., Kent, S., et al. 2002, *AJ*, 123, 2121
- Sneden, C. 1973, Ph.D. Thesis, Univ. Texas at Austin
- Spite, M., Pasquini, L., & Spite, F. 1994, *A&A*, 290, 217
- Steenbock, W., & Holweger, H. 1984, *A&A*, 130, 319
- Stehlé, C., & Hutcheon, R. 1999, *A&AS*, 140, 93
- Strauss, M., & Gunn, J. E. 2001, Technical Note available from <http://www.sdss.org/dr3/instruments/imager>
- Thévenin, F. 1998, *Chemical Abundances in Late-Type Stars. VizieR On-line Data Catalog: III/193*
- Thévenin, F., & Idiart, T. P. 1999, *ApJ*, 521, 753
- Tull, R. G., MacQueen, P. J., Sneden, C., & Lambert, D. L. 1995, *PASP*, 107, 251
- Vandenberg, D. A., & Stetson, P. B. 1991, *AJ*, 102, 1043
- Vandenberg, D. A., Swenson, F. J., Rogers, F. J., et al. 2000, *ApJ*, 532, 430
- Welty, D. E., Hobbs, L. M., & Kulkarni, V. P. 1994, *ApJ*, 436, 152
- Wheeler, J. C., Sneden, C., & Truran, J. W. 1989, *ARA&A*, 27, 279
- Zhou, X., Jiang, Z., Xue, S., et al. 2001, *ChJAA*, 1, 372

Online Material

Table 2. Iron line data. Γ and α are the Van der Waals *FWHM* per perturber at 10 000 K and velocity parameter, respectively. The damping constants for the lines marked with a † correspond to the modified Unsöld approximation. The last column gives the equivalent widths measured in the spectrum of BD +17 4708.

Wavelength Å	Species	E.P. eV	$\log gf$	$\log \Gamma$ rad cm ³ s ⁻¹	$(1 - \alpha)/2$	<i>EW</i> mÅ
4630.120	Fe I	2.279	-2.52	-7.518	0.373	7.0
4745.800	Fe I	3.654	-1.27	-7.356	0.300 †	8.6
4939.686	Fe I	0.859	-3.34	-7.748	0.377	23.9
4994.129	Fe I	0.915	-3.07	-7.744	0.377	28.0
5012.068	Fe I	0.859	-2.64	-7.751	0.377	53.0
5044.211	Fe I	2.851	-2.03	-7.280	0.381	8.3
5051.634	Fe I	0.915	-2.79	-7.746	0.377	42.3
5079.740	Fe I	0.990	-3.22	-7.739	0.378	20.1
5110.413	Fe I	0.000	-3.76	-7.826	0.373	42.4
5123.720	Fe I	1.011	-3.07	-7.739	0.378	26.0
5127.359	Fe I	0.915	-3.31	-7.749	0.377	19.9
5150.839	Fe I	0.990	-3.00	-7.742	0.377	23.0
5151.911	Fe I	1.011	-3.32	-7.740	0.377	17.3
5166.282	Fe I	0.000	-4.20	-7.827	0.373	21.2
5171.596	Fe I	1.485	-1.78	-7.688	0.373	63.4
5194.941	Fe I	1.557	-2.08	-7.680	0.373	45.1
5216.273	Fe I	1.608	-2.14	-7.674	0.372	39.4
5227.189	Fe I	1.557	-1.23	-7.681	0.373	90.1
5228.376	Fe I	4.220	-1.19	-7.233	0.361	4.4
5253.461	Fe I	3.283	-1.57	-7.203	0.386	6.2
5307.360	Fe I	1.608	-2.98	-7.678	0.373	11.8
5322.041	Fe I	2.279	-2.89	-7.600	0.382	4.2
5328.531	Fe I	1.557	-1.85	-7.685	0.374	62.0
5332.899	Fe I	1.557	-2.78	-7.685	0.374	16.0
5341.023	Fe I	1.608	-1.95	-7.679	0.373	52.5
5371.489	Fe I	0.958	-1.65	-7.753	0.376	95.9
5373.708	Fe I	4.473	-0.74	-7.123	0.359	6.5
5397.127	Fe I	0.915	-1.99	-7.759	0.375	81.7
5429.696	Fe I	0.958	-1.88	-7.755	0.376	87.8
5432.947	Fe I	4.445	-0.94	-7.153	0.360	7.2
5434.523	Fe I	1.011	-2.12	-7.750	0.377	72.5
5473.900	Fe I	4.154	-0.72	-7.266	0.380	8.4
5497.516	Fe I	1.011	-2.85	-7.752	0.376	41.0
5501.465	Fe I	0.958	-3.04	-7.757	0.375	32.4
5506.779	Fe I	0.990	-2.80	-7.754	0.376	42.1
5543.935	Fe I	4.217	-1.04	-7.263	0.381	5.1
5638.262	Fe I	4.220	-0.77	-7.270	0.382	6.8
5701.544	Fe I	2.559	-2.22	-7.576	0.382	8.5
5905.671	Fe I	4.652	-0.69	-7.144	0.359	6.0
5930.179	Fe I	4.652	-0.17	-7.149	0.359	24.8
5934.654	Fe I	3.928	-1.07	-7.153	0.377	7.6
6003.012	Fe I	3.881	-1.06	-7.181	0.380	7.8
6027.050	Fe I	4.076	-1.09	-7.397	0.300 †	6.3
6056.004	Fe I	4.733	-0.40	-7.130	0.357	4.7
6170.507	Fe I	4.795	-0.38	-7.119	0.355	6.0
6200.313	Fe I	2.608	-2.44	-7.588	0.382	5.0
6213.430	Fe I	2.223	-2.48	-7.691	0.368	8.9
6232.641	Fe I	3.654	-1.22	-7.498	0.300 †	7.9
6265.133	Fe I	2.176	-2.55	-7.699	0.369	11.2
6344.148	Fe I	2.433	-2.92	-7.620	0.377	3.9
6419.949	Fe I	4.733	-0.24	-7.193	0.363	12.0
6609.110	Fe I	2.559	-2.69	-7.610	0.377	4.2
6750.152	Fe I	2.424	-2.62	-7.608	0.380	6.9
6841.338	Fe I	4.607	-0.71	-7.258	0.367	5.7
6855.162	Fe I	4.558	-0.74	-7.347	0.300 †	5.4
7090.383	Fe I	4.230	-1.11	-7.165	0.376	5.0
4620.521	Fe II	2.828	-3.21	-7.878	0.347	7.4
4629.339	Fe II	2.807	-2.28	-7.886	0.372	42.0
5197.577	Fe II	3.230	-2.22	-7.881	0.377	32.5
5234.625	Fe II	3.221	-2.18	-7.881	0.376	38.0
5264.812	Fe II	3.230	-3.13	-7.875	0.350	7.1
6432.680	Fe II	2.891	-3.57	-7.899	0.398	5.6
6516.081	Fe II	2.891	-3.31	-7.899	0.399	8.8

Table 3. As in Table 2 for the O, Mg, Si, and Ca lines. Equivalent widths are given for all but the strong Mg I *b* lines.

Wavelength Å	Species	E.P. eV	$\log gf$	$\log \Gamma$ rad cm ³ s ⁻¹	$(1 - \alpha)/2$	<i>EW</i> mÅ
7771.944	O I	9.146	0.37	-7.469	0.383	38.2
7774.166	O I	9.146	0.22	-7.469	0.383	31.7
7775.388	O I	9.146	0.00	-7.469	0.383	22.9
4571.096	Mg I	0.000	-5.39	-7.645	0.377	19.4
5167.321	Mg I	2.709	-0.86	-7.267	0.381	—
5172.684	Mg I	2.712	-0.38	-7.267	0.381	—
5183.604	Mg I	2.717	-0.16	-7.267	0.381	—
5711.100	Mg I	4.346	-1.67	-7.218	0.300 †	17.6
5708.397	Si I	4.954	-1.37	-7.183	0.300 †	10.0
5948.540	Si I	5.082	-1.13	-7.169	0.300 †	12.0
7918.382	Si I	5.954	-0.51	-7.010	0.300 †	10.3
7932.348	Si I	5.964	-0.37	-7.006	0.300 †	10.5
4526.928	Ca I	2.709	-0.42	-7.021	0.300 †	15.8
4578.551	Ca I	2.521	-0.56	-7.125	0.300 †	18.3
5512.980	Ca I	2.933	-0.30	-7.269	0.300 †	16.7
6166.439	Ca I	2.521	-0.90	-7.146	0.372	11.3
6169.042	Ca I	2.523	-0.54	-7.146	0.372	21.0
6169.563	Ca I	2.526	-0.27	-7.145	0.372	30.6
6439.075	Ca I	2.526	0.47	-7.569	0.379	69.4
6471.662	Ca I	2.526	-0.59	-7.570	0.380	24.4
6493.781	Ca I	2.521	0.14	-7.571	0.381	54.8
6499.650	Ca I	2.523	-0.59	-7.571	0.381	18.1

Appendix A: Comparison with the literature

Here we compare the atmospheric parameters derived in this paper for BD +17 4708 with those given in the literature (Table 1), with the exception of Peterson (1981), which is not a CCD-based paper. For the absolute iron abundance (A_{Fe}) comparison, corrections due to the different solar iron abundances adopted in each study and effective temperature difference effects (Fe I lines only) are taken into account. For the latter we adopt a correction of 0.2 dex per 300 K (6.67×10^{-4} dex K^{-1} , according to Fig. 9) when necessary. In each case, “our” A_{Fe} value refers to the abundance we would derive with the parameters adopted by each author or group.

- *Rebolo et al. (1988)* adopted a temperature scale similar to that used by Peterson (1981), which is coupled to older Kurucz models by photometric calibrations based essentially on synthetic photometry, but with different color calibrations. They derive $T_{\text{eff}} = 5890$ K. Their $\log g = 4.0$ was obtained from photometric calibrations based on Strömgren photometry. Only one Fe I line was used to derive their $A_{\text{Fe}} = 5.80$. We confirmed the accuracy of the EW given in their paper and for this line only we derive the exact same abundance when using the Rebolo et al. parameters.
- *Magain (1989)* used a photometric calibration based on the IRFM (Magain 1987) to derive $T_{\text{eff}} = 5960$ K. This relatively low IRFM T_{eff} is due to the assumption of zero reddening. The $\log g = 3.40$ derived in this work is too low and it does not satisfy ionization equilibrium with our line data when the low T_{eff} is adopted. Some, but not all, the gf values used in this work are based on a solar analysis. They derive $A_{\text{Fe}} = 5.75$, which is about 0.05 dex lower than our result for the Fe I lines.
- *Axer et al. (1994)* inferred their $T_{\text{eff}} = 6100$ K from model fitting of the Balmer lines. Note that their high $\log g = 4.4$, obtained by forcing ionization equilibrium of Fe lines, is reasonably expected for the temperature adopted. They obtain $A_{\text{Fe}} = 6.09$ while for their T_{eff} our Fe I lines suggest $A_{\text{Fe}} = 5.90$. Axer et al. noticed that due to systematic differences in their EW measurements compared to at least two previous studies, their abundances are probably overestimated by about 0.15 dex. The S/N in this study is significantly lower than in most others. If we correct for this likely error in the EW measurements, then $A_{\text{Fe}} = 5.94$, in good agreement with our result. However, the gf values used by these authors were determined using the solar spectrum so the good agreement may be fortuitous.
- *Spite et al. (1994)* do not give enough details to make a fair comparison. Their $T_{\text{eff}} = 5950$ K and $\log g = 3.30$ values are from the excitation and ionization balance conditions, but no details are given about the line list and atomic data. No solar A_{Fe} is given either.
- *Thévenin & Idiart (1999)* used the Thévenin (1998) catalog as the source for their LTE parameters but no details on their determination are given, except that it is a re-analysis of literature data. They derive non-LTE corrections to the Fe abundances, which amount to about 0.2 dex in the case of BD +17 4708. According to the authors, only the Fe I lines suffer from significant deviations from LTE. With their non-LTE corrections, the iron abundance increases from $A_{\text{Fe}} = 5.71$ to 5.92. Our LTE abundance for their T_{eff} is $A_{\text{Fe}} = 5.81$, from both Fe I and Fe II lines (within 0.02 dex). The 0.1 dex difference in the LTE abundance is likely due to the use of solar gf values in their work. As it is discussed in Sect. 3.6, the increase in the Fe I abundance due to the non-LTE

effects predicted by these authors worsens the ionization balance problem we find.

- *Boesgaard et al. (1999)* used two T_{eff} scales, those by King (1993, K93) and Carney (1983a,b; C83), which result in 6091 K and 5956 K, respectively. The former is based on the modeling of the $H\alpha$ line while the second is essentially the Peterson (1981) T_{eff} scale. The low T_{eff} obtained in this way may be due to several factors, for example: 1) missing opacity in older Kurucz models which leads to overestimated UV and visible fluxes and thus lower T_{eff} to match the observations, 2) metallicity effects not properly accounted for in the T_{eff} vs. color calibrations, which generally result in low temperatures for metal-poor stars if the calibration is constructed mainly with solar metallicity stars, 3) the zero point correction to the T_{eff} scale. Their $[\text{Fe}/\text{H}]$ values have been taken from the literature but put onto the same scale by using the same solar iron abundance. They find $A_{\text{Fe}} = 5.78$ with the K93 scale and $A_{\text{Fe}} = 5.70$ with the C83 scale. These values are both 0.10 dex larger than ours.
- *Fulbright (2000)* performed a classical spectroscopic abundance analysis, deriving T_{eff} from the excitation equilibrium of Fe I lines condition and then setting $\log g$ from the ionization balance condition using Fe II lines. The process is iterative but it starts with the T_{eff} estimate. Given that $\log g$ has a smaller effect on the Fe I abundances, the resulting temperatures and metallicities are mostly affected by errors in the Fe I line modeling. The complete line list used in this study is published and a throughout comparison can be made. In fact, we reproduced this analysis using the same models (Kurucz overshoot) and atomic data. Our resulting A_{Fe} vs. EP relations are shown in Fig. A.1. The gf values given by Fulbright have been empirically corrected so it is not surprising to find a smaller scatter compared to our results (we remind the reader that we avoided this type of corrections given that they may artificially reduce the impact of model uncertainties). As shown in Fig. A.1, with the T_{eff} adopted by Fulbright (6025 K), a small trend with EP still remains but it disappears for $T_{\text{eff}} = 6190$ K. In Fig. A.1 we also show the slope of the A_{Fe} vs. EP trends (ϵ) as a function of T_{eff} (for comparison purposes we also show our ϵ values). This T_{eff} increase degrades the almost perfect ionization balance obtained with $T_{\text{eff}} = 6025$ K (where the Fe I and Fe II abundances agree within 0.03 dex compared to a difference of about 0.08 dex with the high T_{eff}). Thus, it seems that the small deviation from excitation balance was sacrificed to almost perfectly satisfy the ionization balance condition. Clearly, the line-to-line scatter in this analysis is still too large as to use the excitation/ionization balance conditions as good $T_{\text{eff}}/\log g$ indicators, i.e., there will be always room to alter the T_{eff} and $\log g$ values by changing the criteria for excitation and ionization balance, which are not going to be satisfied simultaneously due to model limitations. Note also that the EP coverage of the Fulbright line list is about 2 eV shorter than ours (at least for the lines that can be reasonably well analyzed). The Fulbright analysis suggests $A_{\text{Fe}} \simeq 5.90$, which is larger by about 0.1 dex than our A_{Fe} , most likely due to the use of Kurucz overshoot instead of no-overshoot models. Despite the empirical corrections, the gf scale of Fulbright is in good agreement with the one used in this work. The use of the Barklem et al. (2000) damping constants instead of the modified Unsöld approximation values used by Fulbright does not change the abundances by more than 0.01 dex given that the lines are relatively weak

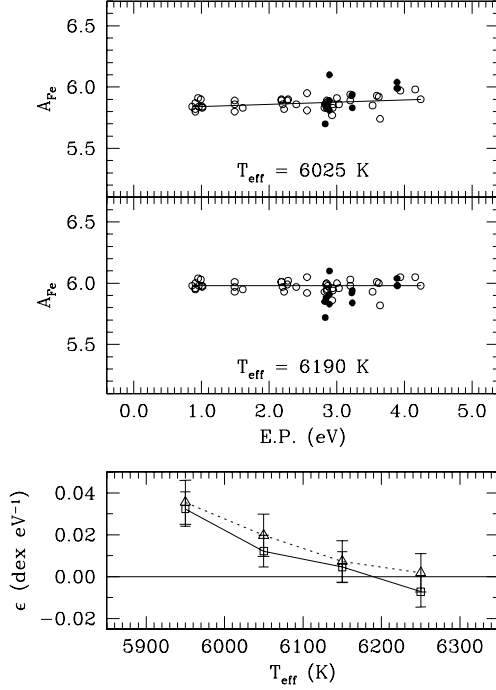


Fig. A.1. *Top panel:* abundance of iron as a function of excitation potential for two different effective temperatures as inferred using the Fulbright (2000) line list. Open circles: Fe I lines, filled circles: Fe II lines. The solid lines are linear fits to the Fe I data only. *Bottom panel:* slope of the A_{Fe} vs. EP trend as a function of T_{eff} using the Fulbright (2000) line list (squares and solid line) and our line list (triangles and dotted line). One-sigma (1σ) errors for the slopes are also shown.

so this does not explain the excitation balance discrepancy. Neither does the use of no-overshoot models.

- *Mishenina et al. (2000)* obtained $T_{\text{eff}} = 5943$ K from the Alonso et al. (1996) IRFM temperature scale and 6000 K from their fitting of models to the $H\alpha$ line. Both values need to be corrected upwards due to reddening and probably observational errors. They derive $A_{\text{Fe}} = 5.90$, in reasonable agreement with our $A_{\text{Fe}} = 5.84$ (after correcting for T_{eff} and solar abundances). Their $\log g = 4.0$ value was inferred by forcing ionization equilibrium of Fe lines. However, their mean Fe I and Fe II abundances have uncertainties of 0.11 and 0.17 dex respectively. Although they use the correct $\log g$, the error bar in their derived value should be very large and the claimed agreement between Fe I and Fe II abundances is questionable.
- *Ryan et al. (2001)* determined $T_{\text{eff}} = 5983$ K by using several color calibrations, including that by Magain (1987), in principle all giving essentially the same T_{eff} . It is interesting, then, to find that even adopting $E(B - V) = 0.01$, they find a low T_{eff} with a T_{eff} scale consistent with that by Magain (1987). This is likely because Ryan et al. explicitly avoided the high temperatures predicted by the IRFM (see Sect. 5.2 in Ryan et al. 1999), claiming an unphysical nature of the color-calibrations by Alonso et al. (1996), which have, however, been recently confirmed by Ramírez & Meléndez (2005b, their Sect. 4.4). The Ryan et al. $[\text{Fe}/\text{H}]$ and $\log g$ values were taken from the literature.
- *Simmerer et al. (2004)* determined T_{eff} from the Alonso et al. (1996) calibrations but with $E(B - V) = 0$, hence the low $T_{\text{eff}} \approx 5941$ K. They inferred $\log g = 3.98$ both from the *Hipparcos* parallax of the star and the ionization balance

condition of iron lines, which is in good agreement with our results for the low T_{eff} . Their iron abundance is $A_{\text{Fe}} = 5.92$ while ours for the same parameters is $A_{\text{Fe}} = 5.82$. The 0.1 dex difference between these abundances is probably due to the use of very weak lines ($EW < 10$ mÅ in most cases), which suffer from errors due to noise and continuum placement. Note that the gf values used in their work are on the same scale as ours (i.e., they were obtained from the same sources), but the lines are not the same.

- *Nissen et al. (2004)* obtained $T_{\text{eff}} = 5943$ K, also from the Alonso et al. (1996) calibrations with zero reddening (as inferred from the Schuster & Nissen 1989 calibration) and $\log g = 3.97$ from the *Hipparcos* parallax. They find $A_{\text{Fe}} = 5.89$, in reasonable agreement with our $A_{\text{Fe}} = 5.82$. Note that they used MARCS instead of Kurucz models. Most of their iron lines are in the blue ($\lambda < 4600$ Å) so it is not possible to make a line-by-line comparison.
- *Meléndez & Ramírez (2004)* used literature values for $[\text{Fe}/\text{H}]$ and $\log g$. Their $T_{\text{eff}} = 6154$ K is from the Ramírez & Meléndez (2005b) IRFM temperature vs. color calibrations, using $E(B - V) \approx 0.02$. Note that for $E(B - V) = 0$, the IRFM temperature vs. color calibrations suggest a lower $T_{\text{eff}} \approx 6050$ K (Fig. 4) while application of the IRFM for this star results in 5955 K (Ramírez & Meléndez 2005a). At $E(B - V) = 0.01$, however, the T_{eff} from the color calibrations is in good agreement with that found in our work.
- *Asplund et al. (2005)* determined $T_{\text{eff}} = 6183$ K from fitting of the wings of the $H\alpha$ line using essentially the same atomic data that we used in Sect. 3.4 but MARCS models instead of Kurucz. The effect of using a different model atmosphere is negligible given that we find a very similar $H\alpha$ temperature (Sect. 3.4). Their $\log g$ value is inferred from the *Hipparcos* parallax of the star. They derive $[\text{Fe}/\text{H}] = -1.51$ ($A_{\text{Fe}} = 5.99$) from both Fe I and Fe II lines, which gave almost the same value for this star (but they find a mean systematic difference of 0.08 dex with the Fe I lines giving lower abundances in their complete sample). The use of the MARCS model adopted by Asplund et al. increases the Fe II abundance by 0.06 dex with respect to the abundance we derived with the Kurucz model but the Fe I abundance remains unchanged. Asplund et al. used only weak Fe I lines with gf values from O’Brian et al. (1991) and Fe II lines for which gf values are from Biémont et al. (1994). When we restrict our line list to lines with these characteristics, the Fe I abundance reduces by 0.03 dex while the Fe II abundance increases by 0.02 dex. Thus, the mean (Fe I–Fe II) difference reduces from 0.15 dex when using our line list, adopted atomic data, and a Kurucz model to 0.03 dex if a MARCS model and a line selection similar to that of Asplund et al. is made.

In summary, the effective temperature differences between the one obtained in this paper and those given in the literature can be explained by ignored reddening, limitations of older models, errors in the observations and basic data in the $H\alpha$ line modeling, and the nature of the classical spectroscopic analysis. In most cases we were able to reproduce the literature abundances with corrections due to solar A_{Fe} and T_{eff} differences. In the other cases, the remaining differences (0.1 dex or less) can be reasonably explained by the atomic data adopted and/or different model atmospheres. This means that the codes for LTE analyses are free of major bugs. Our A_{Fe} values, with conservative error bars, are very robust given that our line list is accurate in an absolute sense.